

This discussion paper is/has been under review for the journal Biogeosciences (BG).
Please refer to the corresponding final paper in BG if available.

Reconstruction of secular variation in seawater sulfate concentrations

T. J. Algeo^{1,2,3}, G. M. Luo^{2,3}, H. Y. Song³, T. W. Lyons⁴, and D. E. Canfield⁵

¹Department of Geology, University of Cincinnati, Cincinnati, Ohio 45221-0013, USA

²State Key Laboratory of Geological Processes and Mineral Resources, China University of Geosciences, Wuhan, 430074, China

³State Key Laboratory of Biogeology and Environmental Geology, China University of Geosciences, Wuhan, 430074, China

⁴Department of Earth Sciences, University of California, Riverside, California 92521-0423, USA

⁵Nordic Center for Earth Evolution (NordCEE) and Institute of Biology, University of Southern Denmark, Campusvej 55, 5230 Odense M, Denmark

Received: 26 July 2014 – Accepted: 23 August 2014 – Published: 10 September 2014

Correspondence to: T. J. Algeo (thomas.algeo@uc.edu)

Published by Copernicus Publications on behalf of the European Geosciences Union.

BGD

11, 13187–13250, 2014

Reconstruction of seawater sulfate

T. J. Algeo et al.

Title Page

Abstract

Introduction

Conclusions

References

Tables

Figures

◀

▶

◀

▶

Back

Close

Full Screen / Esc

Printer-friendly Version

Interactive Discussion



Abstract

Long-term secular variation in seawater sulfate concentrations ($[SO_4^{2-}]_{sw}$) is of interest owing to its relationship to the oxygenation history of Earth's surface environment, but quantitative approaches to analysis of this variation remain underdeveloped. In this study, we develop two complementary approaches for assessment of the $[SO_4^{2-}]$ of ancient seawater and test their application to reconstructions of $[SO_4^{2-}]_{sw}$ variation since the late Neoproterozoic Eon (< 650 Ma). The first approach is based on two measurable parameters of paleomarine systems: (1) the S-isotope fractionation associated with microbial sulfate reduction (MSR), as proxied by $\Delta^{34}S_{CAS-PY}$, and (2) the maximum rate 5 of change in seawater sulfate, as proxied by $\partial\delta^{34}S_{CAS}/\partial t$ (max). This "rate method" yields an estimate of the maximum possible $[SO_4^{2-}]_{sw}$ for the time interval of interest, although the calculated value differs depending on whether an oxic or an anoxic ocean model is inferred. The second approach is also based on $\Delta^{34}S_{CAS-PY}$ but evaluates this parameter against an empirical MSR trend rather than a formation-specific 10 $\partial\delta^{34}S_{CAS}/\partial t$ (max) value. The MSR trend represents the relationship between fractionation of cogenetic sulfate and sulfide (i.e., $\Delta^{34}S_{sulfate-sulfide}$) and ambient dissolved sulfate concentrations in 81 modern aqueous systems. This "MSR-trend method" is 15 thought to yield a robust estimate of mean seawater $[SO_4^{2-}]$ for the time interval of interest. An analysis of seawater sulfate concentrations since 650 Ma suggests that $[SO_4^{2-}]_{sw}$ was low during the late Neoproterozoic (< 5 mM), rose sharply across the Ediacaran/Cambrian boundary (to ~ 5–10 mM), and rose again during the Permian to 20 levels (~ 10–30 mM) that have varied only slightly since 250 Ma. However, Phanerozoic seawater sulfate concentrations may have been drawn down to much lower levels (~ 1–4 mM) during short (\lesssim 2 Myr) intervals of the Cambrian, Early Triassic, Early Jurassic, 25 and possibly other intervals as a consequence of widespread ocean anoxia, intense MSR, and pyrite burial. The procedures developed in this study offer potential for future high-resolution quantitative analyses of paleoseawater sulfate concentrations.

BGD

11, 13187–13250, 2014

Reconstruction of seawater sulfate

T. J. Algeo et al.

Title Page	
Abstract	Introduction
Conclusions	References
Tables	Figures
◀	▶
◀	▶
Back	Close
Full Screen / Esc	
Printer-friendly Version	
Interactive Discussion	



1 Introduction

Oceanic sulfate plays a key role in the biogeochemical cycles of S, C, O and Fe (Canfield, 1998; Lyons and Gill, 2010; Halevy et al., 2012; Planavsky et al., 2012). For example, > 50 % of organic matter and methane in marine sediments is oxidized via

5 processes linked to microbial sulfate reduction (MSR) (Jørgensen, 1982; Valentine, 2002). At a concentration of ~ 29 mM in the modern ocean, sulfate is the second most abundant anion in seawater (Millero, 2005). Its concentration is an important proxy for seawater chemistry and the oxidation state of the Earth's atmosphere and oceans (Kah et al., 2004; Johnston, 2011).

10 Although there is broad agreement that seawater sulfate concentrations have increased through time, the history of its accumulation remains poorly known in detail. Archean and Early Proterozoic oceans are thought to have had very limited sulfate inventories (< 200 µM), as implied by small degrees of sulfate-sulfide and mass-independent S-isotope fractionation (Shen et al., 2001; Strauss, 2003; Farquhar et al., 2007; Adams et al., 2010; Johnston, 2011; Owens et al., 2013; Luo et al., 2014). The accumulation of atmospheric O₂ during Great Oxidation Event (GOE) I (~ 2.3– 15 2.0 Ga; Holland, 2002; Bekker et al., 2004; Guo et al., 2009) is thought to have resulted in a long-term increase in seawater sulfate concentrations (Canfield and Raiswell, 1999; Canfield et al., 2007; Kah et al., 2004; Fike et al., 2006; Schröder et al., 2008; 20 Planavsky et al., 2012; Reuschel et al., 2012). However, this increase was probably not monotonic and declines in pO₂ may have resulted in one or more seawater sulfate minima between ~ 1.9 and 0.6 Ga (Planavsky et al., 2012; Luo et al., 2014). Estimates of Phanerozoic seawater sulfate concentrations are uniformly higher, although there is no consensus regarding exact values. Fluid inclusion data yielded estimates of ~ 10 to 30 mM for most of the Phanerozoic (Horita et al., 2002; Lowenstein et al., 2003). However, recent S-isotope studies have modeled concentrations as low as ~ 1–5 mM during portions of the Cambrian, Triassic, Jurassic, and Cretaceous (Wortmann and Chernyavsky, 2007; Adams et al., 2010; Luo et al., 2010; Gill et al., 2011a, b; Newton 25

BGD

11, 13187–13250, 2014

Reconstruction of seawater sulfate

T. J. Algeo et al.

[Title Page](#)

[Abstract](#)

[Introduction](#)

[Conclusions](#)

[References](#)

[Tables](#)

[Figures](#)

◀

▶

◀

▶

[Back](#)

[Close](#)

[Full Screen / Esc](#)

[Printer-friendly Version](#)

[Interactive Discussion](#)



et al., 2011; Owens et al., 2013; Song et al., 2014), and a recent marine S-cycle model yielded low concentrations (< 10 mM) for the entire Cretaceous and Early Cenozoic before a rise to near-modern levels at ~ 40 Ma (Wortmann and Paytan, 2012).

Here, we develop two approaches for quantitative analysis of seawater sulfate concentrations ($[SO_4^{2-}]_{SW}$) in paleoceanographic systems. The first method calculates a maximum possible $[SO_4^{2-}]_{SW}$ based on a combination of two parameters that are readily measurable in most paleoceanographic systems: (1) the S-isotope fractionation between co-genetic sedimentary sulfate and sulfide ($\Delta^{34}S_{CAS-PY}$), and (2) the maximum observed rate of variation in seawater sulfate $\delta^{34}S$ ($\partial \delta^{34}S_{CAS} / \partial t$). This “rate method” is an extension of earlier modeling work by Kump and Arthur (1999), Kurtz et al. (2003), Kah et al. (2004), Bottrell and Newton (2006), and Gill et al. (2011a, b). The second approach yields an estimate of mean seawater $[SO_4^{2-}]$ based on an empirical relationship between $\Delta^{34}S_{CAS-PY}$ and ambient dissolved sulfate concentrations in 81 modern aqueous systems (the MSR trend). This “MSR-trend method” is thus based on an updated version of the fractionation relationship that was quantified by Habicht et al. (2002; their Fig. 1). Whereas earlier analyses commonly made qualitative assessments of paleo-seawater $[SO_4^{2-}]$ (e.g., Chu et al., 2007), the significance of our methodology is that the $[SO_4^{2-}]$ of ancient seawater can be quantitatively constrained as a function of measurable sediment parameters and empirical fractionation relationships.

We fully recognize that the marine sulfur cycle is controlled by myriad factors, many of which are only now coming to light thanks to detailed field and laboratory studies, and that not all such influences can be thoroughly considered and accommodated in the present study. While acknowledging the complexity of the sulfur cycle, this paper attempts to identify broad first-order trends that potentially transcend these diverse influences and that are robust over significant intervals of geologic time. Our ultimate goal is to generate useful approximations of the long-term history of sulfate in the ocean. Our results suggest that large-scale empirical relationships may exist that are not highly sensitive to local controls such as rates of MSR, syngenetic vs. diagenetic pyrite formation, and strain-specific isotopic behavior, among others. We envision such

BGD

11, 13187–13250, 2014

Reconstruction of seawater sulfate

T. J. Algeo et al.

[Title Page](#)

[Abstract](#)

[Introduction](#)

[Conclusions](#)

[References](#)

[Tables](#)

[Figures](#)

◀

▶

◀

▶

[Back](#)

[Close](#)

[Full Screen / Esc](#)

[Printer-friendly Version](#)

[Interactive Discussion](#)



local influences, as they become more completely understood, being mapped onto, and thus integrated with, the broad first-order relationships documented herein.

BGD

11, 13187–13250, 2014

2 Methods of modeling paleo-seawater sulfate concentrations

2.1 The rate method

- 5 The marine S cycle has a limited number of fluxes with well-defined S-isotope ranges (Holser et al., 1989; Canfield, 2004; Bottrell and Newton, 2006) and, thus, is amenable to analysis through modeling (e.g., Halevy et al., 2012). Subaerial weathering yields a riverine sulfate source flux (F_Q) of $\sim 10 \times 10^{13} \text{ g yr}^{-1}$ with an average $\delta^{34}\text{S}$ of $\sim +6\text{\textperthousand}$, which is significantly lighter than the modern seawater sulfate $\delta^{34}\text{S}$ of $+20\text{\textperthousand}$. Sulfate
10 is removed to the sediment either in an oxidized state, as carbonate-associated sulfate (CAS) or evaporite deposits, or in a reduced state, mainly as FeS or FeS₂. The oxidized sink has a flux (F_{EVAP}) of $\sim 6 \times 10^{13} \text{ g yr}^{-1}$ with a S-isotopic composition that closely mimics that of coeval seawater ($\Delta^{34}\text{S}_{\text{SW-EVAP}}$ of -4 to 0\textperthousand). The reduced sink has a flux (F_{PY}) of $\sim 4 \times 10^{13} \text{ g yr}^{-1}$ with a composition that characteristically shows
15 a large negative fractionation relative to coeval seawater ($\Delta^{34}\text{S}_{\text{SW-PY}}$ of ~ 30 to $60\text{\textperthousand}$; Habicht and Canfield, 1997). Secular variation in seawater sulfate $\delta^{34}\text{S}$ is mainly due to changes in the relative size of the sink fluxes, with increasing (decreasing) burial of pyrite relative to sulfate leading to more (less) ³⁴S-enriched seawater sulfate (Holser et al., 1989; Bottrell and Newton, 2006; Halevy et al., 2012).
- 20 We adapted the models of Kurtz et al. (2003) and Kah et al. (2004) in order to calculate ancient seawater sulfate concentrations ($[\text{SO}_4^{2-}]_{\text{SW}}$) based on two parameters: (1) S-isotope fractionation between cogenetic sedimentary sulfate and sulfide ($\Delta^{34}\text{S}_{\text{sulfate-sulfide}}$, as proxied by $\Delta^{34}\text{S}_{\text{CAS-PY}}$), and (2) the maximum observed rate of variation in seawater sulfate S isotopes ($\partial\delta^{34}\text{S}_{\text{SO}_4}/\partial t(\text{max})$, as proxied by
25 $\partial\delta^{34}\text{S}_{\text{CAS}}/\partial t(\text{max})$) (Fig. 1). Rates of isotopic change for seawater sulfate are given

[Title Page](#)

[Abstract](#)

[Introduction](#)

[Conclusions](#)

[References](#)

[Tables](#)

[Figures](#)

◀

▶

◀

▶

[Back](#)

[Close](#)

[Full Screen / Esc](#)

[Printer-friendly Version](#)

[Interactive Discussion](#)



by:

$$\partial \delta^{34}\text{S}_{\text{CAS}} / \partial t = \left((F_Q \times \Delta^{34}\text{S}_{\text{Q-SW}}) - (F_{\text{PY}} \times \Delta^{34}\text{S}_{\text{CAS-PY}}) \right) / M_{\text{SW}} \quad (1)$$

where $F_Q \times \Delta^{34}\text{S}_{\text{Q-SW}}$ is the flux-weighted difference in the isotopic compositions of the source flux and seawater (SW), $F_{\text{PY}} \times \Delta^{34}\text{S}_{\text{CAS-PY}}$ is the flux-weighted difference in the isotopic compositions of the reduced-S sink flux and seawater, and M_{SW} is the mass of seawater sulfate. The full expression represents the time-integrated influence of the source and sink fluxes on seawater sulfate $\delta^{34}\text{S}$. The maximum possible rate of change in the sulfur isotopic composition of seawater sulfate is attained when one of the fluxes (e.g., the source flux, as in Eq. 2) goes to zero:

$$\partial \delta^{34}\text{S}_{\text{CAS}} / \partial t(\text{max}) = F_{\text{PY}} \times \Delta^{34}\text{S}_{\text{CAS-PY}} / M_{\text{SW}} \quad (2)$$

Reorganization of this equation allows calculation of a maximum seawater sulfate concentration from measured values of $\Delta^{34}\text{S}_{\text{CAS-PY}}$ and $\partial \delta^{34}\text{S}_{\text{CAS}} / \partial t(\text{max})$:

$$M_{\text{SW}} = k_1 \times F_{\text{PY}} \times \Delta^{34}\text{S}_{\text{CAS-PY}} / (\partial \delta^{34}\text{S}_{\text{CAS}} / \partial t(\text{max})) \quad (3)$$

$$[\text{SO}_4^{2-}]_{\text{SW}}(\text{max}) = k_2 \times M_{\text{SW}} \quad (4)$$

where k_1 is a unit-conversion constant equal to 10^6 , and k_2 is a constant relating the mass of seawater sulfate to its molar concentration that is equal to $2.15 \times 10^{-20} \text{ mM g}^{-1}$.

Kah et al. (2004) used $F_{\text{PY}} = 10 \times 10^{13} \text{ g yr}^{-1}$, which is the total sink flux for modern seawater sulfate, in order to model $\partial \delta^{34}\text{S}_{\text{CAS}} / \partial t(\text{max})$. While this may be appropriate for intervals of widespread euxinia in the global ocean, $F_{\text{PY}} = 4 \times 10^{13} \text{ g yr}^{-1}$ (i.e., the modern value) may better represent intervals with well-oxygenated oceans in which the sinks of sulfate S and pyrite S are subequal (Fig. 1). For values of $\Delta^{34}\text{S}_{\text{CAS-PY}}$ and $\partial \delta^{34}\text{S}_{\text{CAS}} / \partial t(\text{max})$ that are potentially representative of the modern ocean (e.g., 35 %

BGD

11, 13187–13250, 2014

Reconstruction of seawater sulfate

T. J. Algeo et al.

[Title Page](#)

[Abstract](#)

[Introduction](#)

[Conclusions](#)

[References](#)

[Tables](#)

[Figures](#)

[◀](#)

[▶](#)

[◀](#)

[▶](#)

[Back](#)

[Close](#)

[Full Screen / Esc](#)

[Printer-friendly Version](#)

[Interactive Discussion](#)



and 1.1‰ Myr^{-1} ; see discussion below), Eq. (3) yields the modern seawater sulfate mass of $M_{\text{SW}} = 1.3 \times 10^{21}\text{ g}$ (assuming $F_{\text{PY}} = 4 \times 10^{13}\text{ g yr}^{-1}$), and Eq. (4) yields the modern seawater sulfate concentration of $\sim 29\text{ mM}$ (Millero, 2005).

Relationships among the model parameters are illustrated in Fig. 1 for $\Delta^{34}\text{S}_{\text{CAS-PY}}$ from 1 to 100‰ (ordinal scale) and for discrete values of $\partial\delta^{34}\text{S}_{\text{CAS}}/\partial t(\text{max})$ ranging from 1 to 100‰ Myr^{-1} (diagonal lines). $[\text{SO}_4^{2-}]_{\text{SW}}$ increases linearly with increasing $\Delta^{34}\text{S}_{\text{CAS-PY}}$ (at constant $\partial\delta^{34}\text{S}_{\text{CAS}}/\partial t(\text{max})$) and decreases linearly with increasing $\partial\delta^{34}\text{S}_{\text{CAS}}/\partial t(\text{max})$ (at constant $\Delta^{34}\text{S}_{\text{CAS-PY}}$). The *observed* maximum $\partial\delta^{34}\text{S}_{\text{CAS}}/\partial t$ is generally smaller than the *theoretical* maximum $\partial\delta^{34}\text{S}_{\text{SO}_4}/\partial t$ because the latter can be achieved only when the source flux of seawater sulfate is reduced (at least transiently) to zero (Kah et al., 2004), which does not routinely occur in nature. As a consequence, estimates of $[\text{SO}_4^{2-}]_{\text{SW}}$ for a given paleomarine system generally are larger than actual seawater sulfate concentrations, so Eq. (4) yields the *maximum likely* $[\text{SO}_4^{2-}]_{\text{SW}}$ for an interval of interest. This outcome is illustrated by a calculation for the modern ocean, using $\Delta^{34}\text{S}_{\text{CAS-PY}}$ of $\sim 30\text{--}60\text{‰}$ (e.g., Canfield and Thamdrup, 1994) and $\partial\delta^{34}\text{S}_{\text{CAS}}/\partial t(\text{max})$ of $\sim 0.5\text{‰ Myr}^{-1}$ (based on the Cenozoic seawater sulfate $\delta^{34}\text{S}$ record; Paytan et al., 1998). These inputs yield $[\text{SO}_4^{2-}]_{\text{SW}}$ (max) values between ~ 40 and 120 mM , which is modestly larger than the actual modern $[\text{SO}_4^{2-}]_{\text{SW}}$ of $\sim 29\text{ mM}$ (Fig. 1). Overestimation of modern $[\text{SO}_4^{2-}]_{\text{SW}}$ is due to the fact that observed $\partial\delta^{34}\text{S}_{\text{CAS}}/\partial t$ values for the Cenozoic are just $< 0.5\text{‰ Myr}^{-1}$ and, thus, have not approached the theoretical maximum for modern seawater ($\sim 1\text{--}2\text{‰ Myr}^{-1}$; Fig. 1). This situation is probably typical of the marine sulfur cycle through time – maximum observed rates of $\partial\delta^{34}\text{S}_{\text{CAS}}/\partial t$ are generally going to be lower than maximum *theoretical* rates because the source flux of sulfur to the oceans has probably never gone to zero (as modeled in Eq. 2).

Reconstruction of seawater sulfate

T. J. Algeo et al.

Title Page

Abstract

Introduction

Conclusions

References

Tables

Figures

◀

▶

◀

▶

Back

Close

Full Screen / Esc

Printer-friendly Version

Interactive Discussion



2.2 The MSR-trend method

An alternative approach to constraining ancient seawater sulfate concentrations is based on empirical relationships with the S-isotope fractionation associated with microbial sulfate reduction (F_{MSR}). We evaluated this relationship by compiling 5 $\Delta^{34}\text{S}_{\text{sulfate-sulfide}}$ and $[\text{SO}_4^{2-}]_{\text{aq}}$ data for 81 examples from modern aqueous systems, including freshwater, brackish, marine, and hypersaline environments (Table A1; cf. Habicht et al., 2002). Each system was classified (1) by salinity, as freshwater (< 10 psu), brackish (10–30 psu), marine (30–40 psu), or hypersaline (> 40 psu; n.b., psu = practical salinity units), and (2) by redox conditions, as oxic or euxinic depending 10 on whether the chemocline was within the sediment or the watermass, respectively.

In the interests of applying uniform criteria to the generation of this dataset, we followed a specific protocol. First, we used only in-situ water-column measurements of $\delta^{34}\text{S}$ for aqueous sulfate. Second, we used in-situ water-column or uppermost 15 sediment-porewater measurements of $\delta^{34}\text{S}$ for aqueous sulfide or, if lacking, measurements of $\delta^{34}\text{S}$ of sedimentary sulfide as a proxy for aqueous sulfide. Because solid-phase sulfides generally exhibit a pronounced shift toward more ^{34}S -enriched compositions under sulfate-limited (e.g., burial) conditions, we used $\delta^{34}\text{S}$ values only from samples taken at or within a few centimeters of the sediment-water interface. Some variation in $\delta^{34}\text{S}$ among cogenetic sedimentary sulfides is common. Pyrite S is 20 generally more ^{34}S -depleted than acid-volatile S (AVS) and organic S because it represents a time-integrated signal that incorporates early-generated, strongly ^{34}S -depleted H₂S (Kaplan et al., 1963; Canfield et al., 1992). On the other hand, AVS tends to have a heavier sulfur isotopic composition, closer to that of the instantaneously generated H₂S at a given sediment depth, because it converts quickly to pyrite with burial (Lyons, 25 1997), and organic S tends to be isotopically heavier possibly owing to fractionations associated with the sulfurization of organic matter (Werne et al., 2000, 2003, 2008). For these reasons, we utilized pyrite rather than AVS or other solid-phase sulfides as a proxy in estimating aqueous sulfide $\delta^{34}\text{S}$. Third, we adopted a modern seawater

[Title Page](#)[Abstract](#)[Introduction](#)[Conclusions](#)[References](#)[Tables](#)[Figures](#)[◀](#)[▶](#)[◀](#)[▶](#)[Back](#)[Close](#)[Full Screen / Esc](#)[Printer-friendly Version](#)[Interactive Discussion](#)

sulfate concentration of 2775 mg L⁻¹ or 28.9 mM (given a seawater density of 1025 kg m⁻³) (Millero, 2005). For non-marine settings, we used measured aqueous sulfate concentrations wherever available. Where unavailable for brackish or hypersaline marine systems, we calculated dissolved sulfate concentration from salinity data:

$$[\text{SO}_4^{2-}] = [\text{SO}_4^{2-}]_{\text{sw}} \times S/S_{\text{sw}} \quad (5)$$

where $[\text{SO}_4^{2-}]$ and S are the sulfate concentration and salinity of the watermass of interest, respectively, and S_{sw} is the salinity of average seawater (35 psu). Some secular variation in the salinity and, hence, aqueous sulfate concentration of non-marine and restricted-marine watermasses is likely, but its potential effect on the $F_{\text{MSR}}\text{-}[\text{SO}_4^{2-}]_{\text{aq}}$ relationship may be limited.

The protocol above produced an internally consistent dataset (Table A1) that exhibits a pronounced relationship between $\Delta^{34}\text{S}_{\text{sulfate-sulfide}}$ and $[\text{SO}_4^{2-}]_{\text{aq}}$ (Fig. 2a). Regression of $\Delta^{34}\text{S}_{\text{sulfate-sulfide}}$ on $[\text{SO}_4^{2-}]_{\text{aq}}$ yields a linear relationship with a strong positive correlation ($r^2 = 0.80$). The trend represents an increase in $\Delta^{34}\text{S}_{\text{sulfate-sulfide}}$ from ~4–6‰ at 0.1 mM to ~30–60‰ at 29 mM (i.e., modern seawater $[\text{SO}_4^{2-}]$). $\Delta^{34}\text{S}_{\text{sulfate-sulfide}}$ appears to peak at $[\text{SO}_4^{2-}]_{\text{aq}}$ of 15–20 mM, with a mean value ~5–10‰ greater than for $[\text{SO}_4^{2-}]_{\text{sw}}$, but this effect is small relative to the overall relationship between $\Delta^{34}\text{S}_{\text{sulfate-sulfide}}$ and $[\text{SO}_4^{2-}]_{\text{aq}}$, and we did not factor it separately into the regression analysis. For hypersaline environments in which $[\text{SO}_4^{2-}]_{\text{aq}} > 29$ mM, $\Delta^{34}\text{S}_{\text{sulfate-sulfide}}$ does not continue to rise but, rather, shows roughly the same range as for modern seawater (Fig. 2a). Finally, we analyzed the data by redox environment and found only minor and statistically insignificant differences between oxic and euxinic settings (n.b., hypersaline environments were not included in this analysis). The distributions of the oxic and euxinic datasets show broad overlap (Fig. 2a), so benthic redox conditions appear to exhibit no discernible influence on the relationship of $\Delta^{34}\text{S}_{\text{sulfate-sulfide}}$ to $[\text{SO}_4^{2-}]_{\text{aq}}$.

Reconstruction of seawater sulfate

T. J. Algeo et al.

[Title Page](#)

[Abstract](#)

[Introduction](#)

[Conclusions](#)

[References](#)

[Tables](#)

[Figures](#)

◀

▶

◀

▶

[Back](#)

[Close](#)

[Full Screen / Esc](#)

[Printer-friendly Version](#)

[Interactive Discussion](#)



Reconstruction of seawater sulfate

T. J. Algeo et al.

[Title Page](#)[Abstract](#)[Introduction](#)[Conclusions](#)[References](#)[Tables](#)[Figures](#)[◀](#)[▶](#)[◀](#)[▶](#)[Back](#)[Close](#)[Full Screen / Esc](#)[Printer-friendly Version](#)[Interactive Discussion](#)

Our analysis demonstrates that a strong relationship exists between F_{MSR} and $[\text{SO}_4^{2-}]_{\text{aq}}$ in natural aqueous systems ($r^2 = 0.80$; Fig. 2a). Our results are similar to, although more linear and more statistically robust than, those reported by Habicht et al. (2002) on the basis of culture experiments. We recognize that there are multiple environmental and physiological controls on fractionation by sulfate reducers (see discussion below), and that under certain natural and experimental conditions the relationship of F_{MSR} to $[\text{SO}_4^{2-}]_{\text{aq}}$ can deviate markedly from that in our dataset. However, the pattern of covariation between F_{MSR} and $[\text{SO}_4^{2-}]_{\text{aq}}$ documented here represents a robust relationship that appears to hold for a wide range of natural environments, reflecting a widespread and possibly ubiquitous influence of $[\text{SO}_4^{2-}]_{\text{aq}}$ on F_{MSR} . Nonetheless, the strength of the $F_{\text{MSR}}\text{-}[\text{SO}_4^{2-}]_{\text{aq}}$ relationship shown in Fig. 2a suggests that it can serve as a basis for evaluating the $[\text{SO}_4^{2-}]_{\text{aq}}$ of ancient seawater. Seawater $[\text{SO}_4^{2-}]$ can be estimated graphically by projecting measured values of $\Delta^{34}\text{S}_{\text{CAS-PY}}$ from the ordinal scale to the MSR trend and then to the abscissa (Fig. 2b), or by using the following empirical equation:

$$[\text{SO}_4^{2-}] = 0.42 \times \Delta^{34}\text{S}_{\text{CAS-PY}} - 0.15 \quad (6)$$

The upper and lower uncertainty limits for estimates of seawater $[\text{SO}_4^{2-}]$ based on this relationship are:

$$[\text{SO}_4^{2-}] = 0.40 \times \Delta^{34}\text{S}_{\text{CAS-PY}} - 0.02 \quad (\text{upper limit}) \quad (7)$$

$$[\text{SO}_4^{2-}] = 0.44 \times \Delta^{34}\text{S}_{\text{CAS-PY}} - 0.28 \quad (\text{lower limit}) \quad (8)$$

In order to account for uncertainties in $\Delta^{34}\text{S}_{\text{CAS-PY}}$ as well as the F_{MSR} regression, estimates of minimum $[\text{SO}_4^{2-}]_{\text{SW}}$ should make use of minimum $\Delta^{34}\text{S}_{\text{CAS-PY}}$ values in combination with the upper uncertainty limit equation (Eq. 7), and estimates of maximum $[\text{SO}_4^{2-}]_{\text{SW}}$ should make use of maximum $\Delta^{34}\text{S}_{\text{CAS-PY}}$ values in combination with the lower uncertainty limit equation (Eq. 8; Fig. 2b).

3 Controls on fractionation by microbial sulfate reducers

The biogeochemical nature of the microbial sulfate reduction (MSR) process and its associated S-isotope fractionations have been extensively investigated in earlier studies. Sulfate reducers preferentially utilize sulfate containing ^{32}S during dissimilatory reduction to hydrogen sulfide in conjunction with the anaerobic decay of organic matter (Kaplan, 1983; Canfield, 2001; Bradley et al., 2011). The exact controls on this isotopic discrimination continue to be a topic of intense debate. The paradigmatic view is that this fractionation is mainly a kinetic effect associated with the rate-limiting step for intracellular sulfate processing, although it is known that fractionation also may accompany sulfate transport across the cell membrane (Rees, 1973; Detmers et al., 2001; Brüchert, 2004; Bradley et al., 2011). The kinetic effect is thought to be dependent on aqueous sulfate concentrations, with substantially larger fractionations associated with $[\text{SO}_4^{2-}]_{\text{aq}} \gtrsim 200 \mu\text{M}$ (Habicht et al., 2002; Gomes and Hurtgen, 2013; but see Canfield, 2001, for a counter example). Rees (1973) proposed a maximum discrimination of 46‰ but the theoretical basis for this value was re-assessed by Brunner and Bernasconi (2005). Recent studies have documented F_{MSR} as large as 66‰ in culture experiments (Sim et al., 2011a) and 72‰ in natural systems (Wortmann et al., 2001; Canfield et al., 2010). Even larger fractionations have been reported but are generally considered to be the result of multistage disproportionation of intermediate-oxidation-state sulfur compounds (Canfield and Thamdrup, 1994).

Investigations of natural and experimental systems have documented a number of additional controls on F_{MSR} . One of the most important controls is f_{SO_4} , i.e., the fraction of remaining dissolved sulfate (Gomes and Hurtgen, 2013). In “open systems” containing a high concentration of dissolved sulfate (e.g., the modern ocean), f_{SO_4} does not vary measurably from 1.0 because the quantity of sulfate converted to sulfide via MSR is a small fraction of the total aqueous sulfate inventory. In this case, the produced sulfide will show the maximum degree of fractionation, which is typically ~30 to 60‰ in modern marine systems (Habicht and Canfield, 1997; Fig. 2a). In contrast, in “closed

Reconstruction of seawater sulfate

T. J. Algeo et al.

[Title Page](#)

[Abstract](#)

[Introduction](#)

[Conclusions](#)

[References](#)

[Tables](#)

[Figures](#)

◀

▶

◀

▶

[Back](#)

[Close](#)

[Full Screen / Esc](#)

[Printer-friendly Version](#)

[Interactive Discussion](#)



systems” in which the aqueous sulfate inventory is limited (e.g., sediment porewaters or low-sulfate freshwater systems), dissolved sulfate concentrations can be substantially reduced or completely depleted through MSR, causing f_{SO_4} to evolve toward zero. As $[\text{SO}_4^{2-}]_{\text{aq}}$ becomes smaller, sulfate reducers utilize a progressively larger fraction of the total dissolved sulfate pool, reducing the effective fractionation to small values (Habicht et al., 2002; Gomes and Hurtgen, 2013). In these settings, the aggregate $\delta^{34}\text{S}$ composition of the produced sulfide approaches that of the original aqueous sulfate inventory, and $\Delta^{34}\text{S}_{\text{sulfate-sulfide}}$ approaches zero (Kaplan, 1983; Habicht et al., 2002). In a macro sense, f_{SO_4} can be proxied by $[\text{SO}_4^{2-}]_{\text{aq}}$, accounting for the strong first-order relationship between the latter parameter and $\Delta^{34}\text{S}_{\text{sulfate-sulfide}}$ ($r^2 = 0.80$; Fig. 2a). However, not all researchers agree on the importance of f_{SO_4} as a control on F_{MSR} (e.g., Leavitt et al., 2013).

Other factors may influence F_{MSR} under certain conditions. First, different dissimilatory reduction pathways yield different isotopic discriminations. Oxidation of organic substrates to CO_2 yields larger fractionations (~30–60‰) than oxidation to acetate (<18‰) (Detmers et al., 2001; Brüchert et al., 2001; Brüchert, 2004). Incomplete oxidation of organic substrates is a feature characteristic of sulfate reducers in hyper-saline environments (Habicht and Canfield, 1997; Oren, 1999; Detmers et al., 2001; Stam et al., 2010) and may account for the somewhat smaller fractionations typically encountered in such environments (Fig. 2a). Second, the type of organic substrate also matters, as ethanol, lactate, glucose, and other compounds yielded a range of fractionations under otherwise similar conditions (Canfield, 2001; Detmers et al., 2001; Kleikemper et al., 2004; Sim et al., 2011b). Third, sulfate reduction rates may also influence F_{MSR} , with higher rates associated with smaller isotopic discriminations (Kaplan and Rittenberg, 1964; Kemp and Thode, 1968; Chambers et al., 1975; Habicht and Canfield, 1996; Brüchert et al., 2001; Canfield, 2001). Recent experiments by Leavitt et al. (2013) showed that F_{MSR} declines rapidly with increasing sulfate reduction rates before leveling off at ~15–20‰ at rates >50 mmol H_2S per unit substrate per day. Habicht and Canfield (2001) hypothesized that F_{MSR} is only incidentally re-

Reconstruction of seawater sulfate

T. J. Algeo et al.

Title Page

Abstract

Introduction

Conclusions

References

Tables

Figures

◀

▶

◀

▶

Back

Close

Full Screen / Esc

Printer-friendly Version

Interactive Discussion



lated to sulfate reduction rates because both are correlated with the disproportionation of intermediate-oxidation-state S compounds by sulfur-oxidizing bacteria, which have probably been present since the Archean (Johnston et al., 2005; Wacey et al., 2010). Finally, temperature has been shown to affect F_{MSR} in some studies (e.g., Canfield et al., 2006) but not others (e.g., Detmers et al., 2001). The influence of temperature on F_{MSR} may operate through the species-specific temperature dependence of enzymes.

Research to date clearly shows that controls on microbial sulfate reduction are complex and incompletely understood. This situation reflects the diverse composition of the microbial communities that process sulfur in the marine environment and the range of isotopic fractionations associated with those processes (Brüchert, 2004). Yet even though multiple environmental and physiological factors influence F_{MSR} , the strength of its relationship to $[\text{SO}_4^{2-}]_{\text{aq}}$, as documented in this study (Fig. 2a), implies that aqueous sulfate concentrations are the dominant first-order control on F_{MSR} , and that other factors such as organic substrate, rates of MSR, and temperature are second-order controls whose effects may be randomized at a larger scale and do not obscure the dominant influence of $[\text{SO}_4^{2-}]_{\text{aq}}$ in most environments. Whether the quantitative form of our $F_{\text{MSR}}\text{-}[\text{SO}_4^{2-}]_{\text{aq}}$ relationship is unique to the present or valid for the geologic past is unclear. Microbial S-cycling processes are thought to have been conservative through time (e.g., Wacey et al., 2010), although lower atmospheric ρO_2 prior to ~ 0.63 Ga may have limited disproportionation of intermediate-oxidation-state sulfur compounds and, thus, the potential for large fractionations (Habicht and Canfield, 2001; Sørensen and Canfield, 2004; Johnston et al., 2005). In the following analysis, we adopt the $F_{\text{MSR}}\text{-}[\text{SO}_4^{2-}]_{\text{aq}}$ relationship of Fig. 2a as a basis for evaluating the $[\text{SO}_4^{2-}]_{\text{aq}}$ of ancient seawater from ~ 0.63 Ga to the present.

Reconstruction of seawater sulfate

T. J. Algeo et al.

[Title Page](#)

[Abstract](#)

[Introduction](#)

[Conclusions](#)

[References](#)

[Tables](#)

[Figures](#)

◀

▶

◀

▶

[Back](#)

[Close](#)

[Full Screen / Esc](#)

[Printer-friendly Version](#)

[Interactive Discussion](#)



4 Estimation of seawater sulfate concentrations since 630 Ma

4.1 General considerations and modeling protocol

The rate and MSR-trend methods of estimating $[SO_4^{2-}]_{sw}$ provide a basis for analysis of long-term variation in seawater sulfate concentrations. Although both methods utilize measured values of $\Delta^{34}S_{\text{sulfate-sulfide}}$ as a proxy for F_{MSR} , they are quasi-independent in having different transform functions. The transform function of the rate method (Eqs. 3 and 4) makes use of observed rates of seawater sulfate S-isotopic variation (i.e., $\partial\delta^{34}S_{\text{CAS}}/\partial t(\text{max})$), whereas that of the MSR-trend method (Eqs. 6–8) makes use of an empirical relationship between F_{MSR} and $[SO_4^{2-}]_{aq}$. The two methods appear to be applicable over approximately the same range of $[SO_4^{2-}]_{sw}$ concentrations. However, their transform functions have different sensitivities to $[SO_4^{2-}]_{sw}$, with that of the MSR-trend method being greater owing to its lower slope ($m = 0.42$; Fig. 2) compared with that of the rate method ($m = 1.0$; Fig. 1). Thus, a combination of both methods may be the most useful approach to constraining ancient seawater $[SO_4^{2-}]$. Because the rate method yields estimates of *maximum* likely $[SO_4^{2-}]_{sw}$, it should generally yield a higher estimated sulfate concentration than the MSR-trend method, which estimates the mean $[SO_4^{2-}]_{sw}$ of the time interval of interest. The pairing of these procedures is thus useful in providing both mean and maximum estimates of paleo-seawater sulfate concentrations. Combining these two methods is also useful in providing a check on the robustness of the results. For example, if the maximum estimate yielded by the rate method is less than the mean estimate yielded by the MSR-trend method, then the results should be considered unreliable.

Both the rate and MSR-trend methods require defined input variables for calculation of paleo-seawater $[SO_4^{2-}]$. For the rate method, a record of secular variation in seawater sulfate $\delta^{34}S$ is needed from which to calculate $\partial\delta^{34}S_{\text{CAS}}/\partial t$. We generated a seawater sulfate $\delta^{34}S$ record for the Phanerozoic by combining published $\delta^{34}S_{\text{CAS}}$ datasets for the Cenozoic (Paytan et al., 1998), Cretaceous (Paytan et al., 2004), and

BGD

11, 13187–13250, 2014

Reconstruction of seawater sulfate

T. J. Algeo et al.

Title Page	
Abstract	Introduction
Conclusions	References
Tables	Figures
	
	
Back	Close
Full Screen / Esc	
Printer-friendly Version	
Interactive Discussion	



pre-Cretaceous (Kampschulte and Strauss, 2004) (Table A2; Fig. 3a). We calculated LOWESS curves for this composite record per the methodology of Song et al. (2014). LOWESS curves were generated at both a low frequency (i.e., 5 Myr steps) and a high frequency (i.e., 1 Myr steps), the latter resulting in less smoothing of the long-term $\delta^{34}\text{S}_{\text{CAS}}$ trend (Fig. 3a). The LOWESS curves were then used to calculate rates of change in seawater sulfate concentrations ($\partial\delta^{34}\text{S}_{\text{SO}_4}/\partial t$) through the Phanerozoic (Fig. 3b). For both the rate and MSR-trend methods, $\Delta^{34}\text{S}_{\text{sulfate-sulfide}}$ is a defined input variable. As a proxy, we utilized the Phanerozoic $\Delta^{34}\text{S}_{\text{CAS-PY}}$ record of Wu et al. (2010). According to this record, $\Delta^{34}\text{S}_{\text{CAS-PY}}$ averaged $30 \pm 3\text{‰}$ from 540 to 300 Ma increased gradually from 30‰ to 45‰ between 300 and 270 Ma, and then fluctuated around $42 \pm 5\text{‰}$ from 270 to 0 Ma (Fig. 3c).

4.2 Long-term variation in seawater sulfate concentrations

Our composite record shows that seawater sulfate $\delta^{34}\text{S}$ was heavy (~30–40‰) during the Ediacaran to Middle Cambrian, then declined steeply during the Late Cambrian to Early Ordovician, and stabilized at intermediate values (~20–30‰) during the Middle Ordovician to Early Devonian (Table A3; Fig. 3a). Sulfate $\delta^{34}\text{S}$ declined further during the Middle Devonian to Early Mississippian, reaching a minimum of ~12–16‰ during the mid-Mississippian to end-Permian. Sulfate $\delta^{34}\text{S}$ then rose sharply to ~20‰ during the Early Triassic, before declining slightly to a local minimum of ~15‰ around the Jurassic–Cretaceous boundary. Sulfate $\delta^{34}\text{S}$ rose slowly during the Cretaceous and early Cenozoic, finishing with a rapid increase from 17‰ to 22‰ at 40–50 Ma, before stabilizing at 21–23‰ during the mid- to late Cenozoic (Fig. 3a). The low-frequency LOWESS curve exhibits low rates of $\delta^{34}\text{S}$ variation, with a mean of $0.25 (\pm 0.17)\text{‰ Myr}^{-1}$ and a maximum of ~ 0.8‰ Myr^{-1} (Fig. 3b). The high-frequency LOWESS curve exhibits somewhat higher rates of $\delta^{34}\text{S}$ variation, with a mean of $0.40 (\pm 0.45)\text{‰ Myr}^{-1}$ and a maximum of ~ 2.5‰ Myr^{-1} (Fig. 3b). Both curves show low rates of seawater sulfate $\delta^{34}\text{S}$ variation during the Late Cretaceous and Cenozoic (the

Title Page	
Abstract	Introduction
Conclusions	References
Tables	Figures
◀	▶
◀	▶
Back	Close
Full Screen / Esc	
Printer-friendly Version	
Interactive Discussion	



“Cenozoic minimum”) and the mid-Mississippian to mid-Permian (the “Late Paleozoic minimum”) and substantially higher rates during other intervals.

Our reconstructions of mean and maximum seawater sulfate concentrations through the Phanerozoic, based respectively on the MSR-trend and rate methods, are shown in Fig. 4. The mean curve suggests that $[SO_4^{2-}]_{sw}$ was low in the late Ediacaran ($\sim 1\text{--}4\text{ mM}$) but rose sharply in the Early Cambrian (to $\sim 3\text{--}15\text{ mM}$) and remained in that range until the Permian. A long, slow rise in $[SO_4^{2-}]_{sw}$ began in the Early Permian and culminated at $\sim 12\text{--}38\text{ mM}$ in the Middle Triassic. Subsequently, $[SO_4^{2-}]_{sw}$ declined slightly until the mid-Cretaceous (to $\sim 7\text{--}25\text{ mM}$) and then rose slightly during the Late Cretaceous to early Cenozoic (to $11\text{--}35\text{ mM}$). The standard deviation range for the mean curve (blue band) suggests an uncertainty of plus or minus a factor of $\sim 2\times$ in the mean estimate, with the magnitude of the uncertainty shrinking modestly from the Cambrian to the present. The modern seawater sulfate concentration of 29 mM falls within the standard deviation range of the mean trend (Fig. 4).

A maximum $[SO_4^{2-}]_{sw}$ curve can be calculated for both the low- and high-frequency Phanerozoic $\delta^{34}S$ records of Fig. 3a. The low- and high-frequency maximum $[SO_4^{2-}]_{sw}$ curves (shown as black and red lines, respectively, in Fig. 4) mirror the upward trend through the Phanerozoic seen in the mean curve and, thus, are consistent with a factor of $\sim 4\times$ increase in seawater sulfate concentrations since the Early Cambrian. Although the maximum $[SO_4^{2-}]_{sw}$ curves exhibit values that are mostly unrealistically large, it is worth noting that (1) these curves represent the maximum possible, not the most likely, concentrations of seawater sulfate; and (2) the smallest values on the maximum curves are more robust constraints on $[SO_4^{2-}]_{sw}$ than the largest values. The second observation is based on the fact that the smallest values derive from the largest measured rates of $\delta^{34}S_{CAS}$ variation (Fig. 3b), i.e., those rates than most closely approach the theoretical maximum, whereas the largest values are associated with intervals of little or no $\delta^{34}S_{CAS}$ variation. Thus, the lower envelope of maximum $[SO_4^{2-}]_{sw}$ values (dashed line, Fig. 4) provides a more useful constraint on seawater sulfate concentrations than the full curve. We also suggest that, although the upper limits on $[SO_4^{2-}]_{sw}$ imposed

Discussion Paper | Reconstruction of seawater sulfate

T. J. Algeo et al.

[Title Page](#)[Abstract](#)[Introduction](#)[Conclusions](#)[References](#)[Tables](#)[Figures](#)[◀](#)[▶](#)[◀](#)[▶](#)[Back](#)[Close](#)[Full Screen / Esc](#)[Printer-friendly Version](#)[Interactive Discussion](#)

by the rate method may have limited utility for assessment of Phanerozoic seawater sulfate, this method may be of greater value in analyzing Archean and Proterozoic seawater sulfate concentrations, which are thought to have been quite low (< 1 mM; Kah et al., 2004; Canfield et al., 2007; Planavsky et al., 2012).

The results of the rate method are dependent on several factors that influence the estimation of rates of seawater sulfate $\delta^{34}\text{S}$ variation. On the one hand, $\partial\delta^{34}\text{S}_{\text{SO}_4}/\partial t(\text{max})$ can be overestimated if there is an increase in $\delta^{34}\text{S}_{\text{CAS}}$ variance due to diagenesis of samples or procedural artifacts during CAS extraction. On the other hand, data smoothing is inherent in LOWESS curve calculation, reducing the variance in high-frequency datasets (cf. Song et al., 2014) and thus resulting in an underestimation of $\partial\delta^{34}\text{S}_{\text{SO}_4}/\partial t(\text{max})$. The conclusion that such smoothing has occurred in generating the LOWESS curve of Fig. 3a is inescapable given the documented existence of a number of short (< 2 Myr) intervals of strongly elevated $\partial\delta^{34}\text{S}_{\text{SO}_4}/\partial t$ rates within the Phanerozoic (Wortmann and Chernyavsky, 2007; Adams et al., 2010; Gill et al., 2011a, b; Newton et al., 2011; Wotte et al., 2012; Owens et al., 2013; Song et al., 2014; see below for further analysis). During these intervals, $\partial\delta^{34}\text{S}_{\text{SO}_4}/\partial t$ ranged from 10 to > 50‰ Myr⁻¹ (Table A4), rates that are considerably higher than peak rates for the long-term $\delta^{34}\text{S}_{\text{CAS}}$ curve (ca. 2–4‰ Myr⁻¹; Fig. 3b). Because lower values for $\partial\delta^{34}\text{S}_{\text{SO}_4}/\partial t(\text{max})$ yield higher maximum estimates of $[\text{SO}_4^{2-}]$ for ancient seawater (Eqs. 3 and 4), smoothing may account for some of the divergence between the mean and maximum trends in Fig. 4. The Phanerozoic appears to be characterized by such short-term episodes of seawater sulfate drawdown, mainly as a consequence of massive evaporite deposition (Wortmann and Paytan, 2012). However, other factors may have contributed to transient changes in the seawater sulfate inventory, e.g., reduced ventilation of marine sediments and a consequent increase in MSR in the aftermath of mass extinction events (Canfield and Farquhar, 2009).

Comparison of our Phanerozoic seawater sulfate concentration curve with previously published estimates reveals similarities and differences (Fig. 5). Most of these records exhibit a local minimum during the Jurassic or Cretaceous, although the absolute es-

Reconstruction of seawater sulfate

T. J. Algeo et al.

Title Page

Abstract

Introduction

Conclusions

References

Tables

Figures

◀

▶

◀

▶

Back

Close

Full Screen / Esc

Printer-friendly Version

Interactive Discussion



imates of $[SO_4^{2-}]$ for this minimum vary widely (~ 2 to 25 mM; our value of 13 mM is close to the median estimate of ~ 10 mM). The various records are also in agreement that seawater sulfate was elevated during the Permian–Triassic, with concentrations of ~ 15–30 mM. The records diverge prior to the Permian, however, with one model (Holser et al., 1989) suggesting high values (30–50 mM) and another model (Berner, 2004) low values (< 2 mM) through the mid-Paleozoic. Our model indicates intermediate sulfate concentrations (5–10 mM) at that time (Fig. 5). The various records also show dissimilar patterns across the Ediacaran–Cambrian boundary, with uniformly high values in the Holser et al. (1989) model and steeply falling values in the Berner (2004) model. The results of the present study favor a steep rise in seawater sulfate at this boundary (see next section for further analysis). Our Phanerozoic seawater sulfate concentration record, along with that of Halevy et al. (2012), is in good agreement with the available fluid-inclusion data (Fig. 5) and, thus, appears generally robust, although it probably does not capture short-term episodes of seawater sulfate drawdown (cf. Wortmann and Paytan, 2012).

Our reconstruction of long-term secular variation in seawater sulfate concentrations shows a strong relationship to first-order Phanerozoic climate cycles (cf. Algeo et al., 2014). In particular, the interval of the Late Paleozoic Ice Age, which lasted from the mid-Mississippian through the mid-Permian, was characterized by a major change in the ocean sulfate reservoir. At that time, minimum values developed for both seawater sulfate $\delta^{34}S$ (~ 12–16 ‰; Fig. 3a) and rates of $\delta^{34}S_{SO_4}$ variation (< 1 ‰ Myr⁻¹; Fig. 3b), accompanied by a concurrent increase in mean sulfate-sulfide fractionation (from < 30 ‰ to > 40 ‰; Fig. 3c). Whether these are general features of seawater sulfate during icehouse climate modes is not entirely certain. A second interval of major continental glaciation during the Late Cretaceous and Cenozoic also shows low rates of $\delta^{34}S_{SO_4}$ variation and an increase in sulfate-sulfide fractionation but, in contrast to the Late Paleozoic, ³⁴S-enriched and relatively stable seawater sulfate $\delta^{34}S$ values (Fig. 3). The greater stability of seawater sulfate $\delta^{34}S$ during the Cenozoic relative to the Late

Reconstruction of seawater sulfate

T. J. Algeo et al.

[Title Page](#)

[Abstract](#)

[Introduction](#)

[Conclusions](#)

[References](#)

[Tables](#)

[Figures](#)

◀

▶

◀

▶

[Back](#)

[Close](#)

[Full Screen / Esc](#)

[Printer-friendly Version](#)

[Interactive Discussion](#)



Paleozoic may be due to a long-term increase in total seawater sulfate mass (Figs. 4 and 5). We hypothesize that the Late Paleozoic was characterized by low rates of pyrite burial (hence, lower $\delta^{34}\text{S}_{\text{SO}_4}$) and a consequent increase in the mass of seawater sulfate (hence, lower $\partial\delta^{34}\text{S}_{\text{SO}_4}/\partial t$) (cf. Halevy et al., 2012). Low rates of pyrite burial at that time may have been due to a combination of lower sea-level elevations (reducing the total shelf area available for sulfate reduction; cf. Halevy et al., 2012; Algeo et al., 2014), enhanced oceanic ventilation (increasing aerobic decay of organic matter), and increased burial of organic matter in low-sulfate freshwater settings, which was linked to the spread of terrestrial floras (DiMichele and Hook, 1992).

4.3 High-frequency variation in seawater sulfate during the Neoproterozoic and Phanerozoic

We applied the rate and MSR-trend methods to an analysis of short-term variation in $[\text{SO}_4^{2-}]_{\text{SW}}$ during selected intervals of the Neoproterozoic and Phanerozoic for which high-resolution $\delta^{34}\text{S}_{\text{CAS}}$ studies are available. For the Neoproterozoic, recent studies have provided S-isotope records from a number of sites globally as well as improved radiometric geochronologic constraints that are needed for the rate method. Based on these studies, we have estimated $\partial\delta^{34}\text{S}_{\text{SO}_4}/\partial t(\text{max})$ for 10 Neoproterozoic units (Table A4; Fig. 6). Radiometric studies of the Doushantuo Formation in South China (Halverson et al., 2005; Zhang et al., 2005, 2008) provided key ages from which we calculated $\partial\delta^{34}\text{S}_{\text{CAS}}/\partial t(\text{max})$ of 5‰ Myr⁻¹ at ~636–633 Ma and 1.3‰ Myr⁻¹ at ~568–551 Ma (McFadden et al., 2008; Li et al., 2010). The Neoproterozoic succession of Sonora, Mexico yielded $\partial\delta^{34}\text{S}_{\text{CAS}}/\partial t(\text{max})$ estimates of 6‰ Myr⁻¹ and 4‰ Myr⁻¹ (Loyd et al., 2012, 2013). The latest Neoproterozoic Zarls Formation (Nama Group) in Namibia and upper Huqf Supergroup in Oman yielded $\partial\delta^{34}\text{S}_{\text{CAS}}/\partial t(\text{max})$ estimates of 20‰ Myr⁻¹ and 40‰ Myr⁻¹, respectively, at 549–547 Ma (Fike and Grotzinger, 2008; Ries et al., 2009). The rate method yielded $[\text{SO}_4^{2-}]_{\text{SW}}$ estimates ranging from < 0.1 to > 100 mM, although the majority fell between ~1 and 10 mM (Table A4). The MSR-



Reconstruction of seawater sulfate

T. J. Algeo et al.

trend method yielded $[\text{SO}_4^{2-}]_{\text{sw}}$ estimates ranging from < 0.1 to 70 mM, with a majority between ~ 1 and 16 mM. Most units exhibit combinations of $\partial \delta^{34}\text{S}_{\text{CAS}} / \partial t(\text{max})$ and $\Delta^{34}\text{S}_{\text{CAS-PY}}$ values that plot close to or slightly below the MSR trend (Fig. 6), yielding $[\text{SO}_4^{2-}]_{\text{sw}}$ estimates for the MSR-trend method that are equal to or somewhat smaller than the rate-based estimates. This pattern conforms to our expectation that the rate method yields maximum estimates of $[\text{SO}_4^{2-}]_{\text{sw}}$. The only anomalous result is for the upper Huqf Supergroup, which yielded a “mean” estimate based on the MSR-trend method (12–45 mM) that is larger than the “maximum” estimate based on the rate method (1.5–8 mM; Table A4).

We also analyzed $[\text{SO}_4^{2-}]_{\text{sw}}$ for a set of 8 units of Cambrian age. These units yielded $\partial \delta^{34}\text{S}_{\text{CAS}} / \partial t(\text{max})$ of 7 to 23‰ Myr⁻¹ for the Early Cambrian, 9 to 20‰ Myr⁻¹ for the Early–Middle Cambrian boundary (EMCB), and 8 to 20‰ Myr⁻¹ for the Late Cambrian SPICE (Table A4; Fig. 7). These ranges are sufficiently similar that they suggest a limited range of seawater $[\text{SO}_4^{2-}]$ variation during the Cambrian. The rate method yielded $[\text{SO}_4^{2-}]_{\text{sw}}$ estimates ranging from < 0.1 to 18 mM, although the majority fell between ~ 1 and 6 mM. The MSR-trend method yielded $[\text{SO}_4^{2-}]_{\text{sw}}$ estimates ranging from < 0.1 to 40 mM, with a majority between ~ 1 and 8 mM. The two methods thus yielded similar estimates of seawater sulfate concentrations, implying that the results are reasonably robust and that the rate method is not yielding unrealistically large values. All units showed sulfate-sulfide fractionations smaller than the Paleozoic mean of 30 ± 5 (Wu et al., 2010), resulting in lower $[\text{SO}_4^{2-}]_{\text{sw}}$ estimates than for the long-term record (Fig. 4). Once again, most units exhibit combinations of $\partial \delta^{34}\text{S}_{\text{CAS}} / \partial t(\text{max})$ and $\Delta^{34}\text{S}_{\text{CAS-PY}}$ values that plot close to or slightly below the MSR trend (Fig. 7). However, two units (the SPICE events in Australia and Nevada) yielded “mean” estimates based on the MSR-trend method that are larger than their “maximum” estimates based on the rate method. The reasons for these anomalous results will be considered below.

Finally, we analyzed a set of 8 Mesozoic units, ranging in age from the Early Triassic to the late Middle Cretaceous (Table A4; Fig. 8). These units yielded

Title Page	
Abstract	Introduction
Conclusions	References
Tables	Figures
◀	▶
◀	▶
Back	Close
Full Screen / Esc	
Printer-friendly Version	
Interactive Discussion	



$\partial\delta^{34}\text{S}_{\text{CAS}}/\partial t(\text{max})$ of 6 to 60‰ Myr⁻¹, with the highest rates during the Early Triassic and Early Jurassic. The rate method yielded $[\text{SO}_4^{2-}]_{\text{sw}}$ estimates ranging from 1.1 to 120 mM, although the majority fell between ~3 and 20 mM. The MSR-trend method yielded $[\text{SO}_4^{2-}]_{\text{sw}}$ estimates ranging from 1 to 110 mM, with a majority between ~30 and 100 mM (Table A4). In contrast to the Neoproterozoic and Cambrian (see above), most Mesozoic units exhibit a narrow spread of $\Delta^{34}\text{S}_{\text{CAS-PY}}$ values that conform with the mean sulfate-sulfide fractionation for the Mesozoic–Cenozoic (Wu et al., 2010; Fig. 8) and that are within the range of values shown by modern marine systems (~30–60; Habicht and Canfield, 1997). As a consequence, the majority of Mesozoic units exhibit the anomalous pattern of having “mean” estimates based on the MSR-trend method that are larger than their “maximum” estimates based on the rate method (Fig. 8).

Ideally, the rate and MSR-trend methods will yield similar $[\text{SO}_4^{2-}]_{\text{sw}}$ estimates, providing support for the correctness of the results, but differing estimates may also provide information. Although this is true of the majority of the units above, a subset of units show deviations that fall into two categories: (1) units with unusually low $\partial\delta^{34}\text{S}_{\text{CAS}}/\partial t(\text{max})$, yielding rate-based estimates of $[\text{SO}_4^{2-}]_{\text{sw}}$ much larger than MSR-trend-based estimates (lower right field, Fig. 9), and (2) units with unusually high $\partial\delta^{34}\text{S}_{\text{CAS}}/\partial t(\text{max})$, yielding rate-based estimates of $[\text{SO}_4^{2-}]_{\text{sw}}$ much smaller than MSR-trend-based estimates (upper left field, Fig. 9). The most likely explanation for the first type of deviation is that the observed $\partial\delta^{34}\text{S}_{\text{CAS}}/\partial t(\text{max})$ for a given unit is much less than its theoretical maximum. This situation can develop whenever the marine sulfur cycle is in equilibrium (i.e., source and sink fluxes in balance), reflecting persistently stable environmental conditions. In this case, the rate-based estimate of $[\text{SO}_4^{2-}]_{\text{sw}}$ would have little relationship to actual $[\text{SO}_4^{2-}]_{\text{sw}}$, although the MSR-trend-based estimate may still be a good proxy for $[\text{SO}_4^{2-}]_{\text{sw}}$. Surprisingly, very few of the analyzed units (Table A4) show a significant deviation of this type, perhaps because the most heavily scrutinized ancient geologic epochs are those with unstable environments.



The second type of deviation, in which $\partial \delta^{34}\text{S}_{\text{CAS}} / \partial t(\text{max})$ is anomalously high, is more common, being present in three units of Neoproterozoic and Cambrian age (Figs. 6 and 7) and no fewer than 7 of 8 units of Mesozoic age (Fig. 8). This pattern does not have a single obvious explanation (as for the first deviation type), and several potential causes warrant consideration. First, $\partial \delta^{34}\text{S}_{\text{CAS}} / \partial t(\text{max})$ may have been overestimated because of problems related to dating inaccuracies, diagenetic artifacts, or analytical uncertainties in measuring $\delta^{34}\text{S}_{\text{CAS}}$. However, the observation that deviations of this type are more common among Mesozoic units (Fig. 8), which are generally better dated and less diagenetically altered than older units (Figs. 6 and 7) suggests that such problems are relatively uncommon and unlikely to be responsible for most of the observed anomalies. Second, the measured $\Delta^{34}\text{S}_{\text{CAS-PY}}$ for a given unit may be unrepresentative, perhaps because of unusually large fractionations during MSR (cf. Habicht et al., 2002; Canfield et al., 2010). This explanation may be applicable to the Pleistocene Mediterranean sapropel of Scheiderich et al. (2010), which exhibits an unusually large $\Delta^{34}\text{S}_{\text{CAS-PY}}$ ($60 \pm 5\text{‰}$; Fig. 8). However, none of the anomalous units of Neoproterozoic, Cambrian, or Mesozoic age exhibits a $\Delta^{34}\text{S}_{\text{CAS-PY}}$ larger than the modern range of $\sim 30\text{--}60$, so elevated sulfate-sulfide fractionation is unlikely as a general explanation. We are therefore inclined to regard these deviations as products of local depositional conditions and to seek an environmentally based mechanism to account for them.

One method of generating the second type of deviation is for sulfate reduction to occur in a restricted-marine basin. In this case, $\Delta^{34}\text{S}_{\text{CAS-PY}}$ will be controlled by seawater $[\text{SO}_4^{2-}]$, which may be identical (or nearly so) to that in the global ocean. However, the total mass of sulfate in a restricted-marine basin will be much less than that in the global ocean, allowing a more rapid evolution of seawater sulfate $\delta^{34}\text{S}$ in response to oceanographic perturbations. We hypothesize that most or all of the type-two deviations in our study units are the product of MSR within semi-restricted marine basins. The Neoproterozoic Ara Group (Huqf Supergroup) of Oman was deposited in a fault-bounded basin in which massive evaporite deposits accumulated (Fike and Grotzinger, 2008). Most of the Mesozoic units showing type-two deviations are also known to have been

Reconstruction of seawater sulfate

T. J. Algeo et al.

[Title Page](#)

[Abstract](#)

[Introduction](#)

[Conclusions](#)

[References](#)

[Tables](#)

[Figures](#)

◀

▶

◀

▶

[Back](#)

[Close](#)

[Full Screen / Esc](#)

[Printer-friendly Version](#)

[Interactive Discussion](#)



deposited in basins exhibiting some degree of watermass restriction. The Triassic–Jurassic European epicontinental sea was broad, shallow, and laced with local tectonic grabens with restricted deepwater circulation (Röhl et al., 2001; Berra et al., 2010). The South Atlantic was only weakly connected to the global ocean during deposition of 5 Aptian (Early Cretaceous) sediments (Wortmann and Chernyavsky, 2007), and restriction of the Atlantic Ocean continued at least through deposition of organic-rich facies at the Cenomanian–Turonian boundary (Owens et al., 2013). The Cretaceous Western Interior Seaway was almost certainly semi-restricted throughout its existence (Adams et al., 2010). The only Mesozoic unit not to show a type-two deviation, the Middle Triassic Bravaisberget Formation of Spitsbergen (Karcz, 2010; Fig. 8), was deposited in 10 the largely unrestricted Boreal Ocean. These examples serve to illustrate the need to understand the hydrography of paleomarine basins in applying the rate method.

Comparison of the $[\text{SO}_4^{2-}]_{\text{sw}}$ estimates for individual Neoproterozoic and Phanerozoic units shown in Figs. 6–8 with the long-term $[\text{SO}_4^{2-}]_{\text{sw}}$ curve in Fig. 4 provides 15 additional insights regarding the history of seawater sulfate mass. With the exception of the Middle Triassic Bravaisberget Formation, all Mesozoic units exhibit MSR-trend-based estimates that overlap the long-term trend but rate-based estimates that fall below it (Fig. 10). As discussed above, we infer that this pattern reflects anomalously high measured $\partial \delta^{34}\text{S}_{\text{CAS}} / \partial t(\text{max})$ values as a consequence of rapid evolution of seawater sulfate $\delta^{34}\text{S}$ within restricted-marine basins of the proto-Atlantic and western Tethys oceans. Cambrian units exhibit a wide range of $[\text{SO}_4^{2-}]_{\text{sw}}$ estimates, although 20 a cluster of results falls just below the long-term trend, with many estimates between 1 and 5 mM (Fig. 10). We infer that either our long-term record (Fig. 4) overestimates $[\text{SO}_4^{2-}]_{\text{sw}}$ for the Cambrian, or the studied units are biased toward low $[\text{SO}_4^{2-}]_{\text{sw}}$. Neoproterozoic units exhibit an even wider range of $[\text{SO}_4^{2-}]_{\text{sw}}$ estimates than Cambrian 25 units and lack any apparent clustering (Fig. 10). We infer that either seawater sulfate concentrations were highly variable during the Neoproterozoic, or problems with rate estimation and sample diagenesis have generated considerable noise in our dataset. We are inclined toward the interpretation of high seawater sulfate variability during the

Reconstruction of seawater sulfate

T. J. Algeo et al.

[Title Page](#)

[Abstract](#)

[Introduction](#)

[Conclusions](#)

[References](#)

[Tables](#)

[Figures](#)

◀

▶

◀

▶

[Back](#)

[Close](#)

[Full Screen / Esc](#)

[Printer-friendly Version](#)

[Interactive Discussion](#)



Neoproterozoic because all but one of the units in Fig. 6 yielded similar $[SO_4^{2-}]_{sw}$ estimates for the MSR-trend and rate methods, suggesting that the calculated values are robust. Previous studies of Neoproterozoic seawater sulfate have generally inferred low (Hurtgen et al., 2002, 2005, 2006; Ries et al., 2009) or monotonically rising concentrations (Halverson and Hurtgen, 2007), but our findings imply a highly unstable marine S cycle with possible rapid fluctuations between high and low seawater sulfate concentrations from ~ 635 to 542 Ma.

5 Conclusions

The two methods developed in this study for quantifying sulfate concentrations in paleo-seawater are complementary and largely independent, providing estimates of maximum and mean $[SO_4^{2-}]_{sw}$ for the time interval of interest. Both techniques make use of $\Delta^{34}S_{CAS-PY}$, i.e., the isotopic fractionation associated with microbial sulfate reduction (MSR). The “rate method” evaluates $[SO_4^{2-}]_{sw}$ as a function of $\partial\delta^{34}S_{CAS}/\partial t(\max)$, i.e., the maximum observed rate of change in seawater sulfate, whereas the “MSR-trend method” makes use of an empirical relationship between the fractionation associated with MSR and ambient aqueous sulfate concentrations. The significance of our quantitative approach is that estimates of paleo-seawater $[SO_4^{2-}]$ can be derived from two readily measurable sedimentary parameters, $\Delta^{34}S_{CAS-PY}$ and $\delta^{34}S_{CAS}/\partial t(\max)$. An analysis of long-term variation in seawater sulfate concentrations since 630 Ma based on these methods suggests that $[SO_4^{2-}]_{sw}$ was low during the late Neoproterozoic (< 5 mM), rose sharply across the Ediacaran/Cambrian boundary (to ~ 5 – 10 mM), and rose again during the Permian to near-modern levels (~ 10 – 30 mM). However, high-resolution $\delta^{34}S_{CAS}$ studies provide evidence of repeated short-term ($\lesssim 2$ Myr) drawdown of seawater sulfate concentrations during the Phanerozoic, in response to massive evaporite deposition and/or reduced sediment ventilation and increased pyrite burial in the aftermath of mass extinctions. The techniques developed in this study

[Title Page](#)[Abstract](#)[Introduction](#)[Conclusions](#)[References](#)[Tables](#)[Figures](#)[◀](#)[▶](#)[◀](#)[▶](#)[Back](#)[Close](#)[Full Screen / Esc](#)[Printer-friendly Version](#)[Interactive Discussion](#)

for quantitative analysis of paleo-seawater $[\text{SO}_4^{2-}]$ should be applicable to sediments of any age provided that (1) fractionation during MSR has been a conservative process through time (i.e., the dominant pathways of sulfur metabolism have not changed greatly), and (2) reasonable time control exists for estimation of rates of $\delta^{34}\text{S}_{\text{CAS}}$ variation. Given a sufficient number of S-isotopic studies of cogenetic sulfate and sulfide, it should ultimately be possible to reconstruct variation in seawater sulfate concentrations throughout Earth history.

Appendix A: Data tables

The primary sulfur isotopic data and model output for this study are given in Tables A1 to A4.

**The Supplement related to this article is available online at
doi:10.5194/bgd-11-13187-2014-supplement.**

Author contribution. T. J. Algeo developed the project concept and modeling methodology, G. M. Luo, H. Y. Song, T. W. Lyons, and D. E. Canfield provided isotopic data, and all authors assisted in drafting the manuscript.

Acknowledgements. Research by T. J. Algeo and T. W. Lyons is supported by the Sedimentary Geology and Paleobiology program of the US National Science Foundation and the NASA Exobiology program. T. J. Algeo also gratefully acknowledges support from the State Key Laboratory of Geological Processes and Mineral Resources, China University of Geosciences, Wuhan (program GPMR201301).

Reconstruction of seawater sulfate

T. J. Algeo et al.

[Title Page](#)

[Abstract](#)

[Introduction](#)

[Conclusions](#)

[References](#)

[Tables](#)

[Figures](#)



[Full Screen / Esc](#)

[Printer-friendly Version](#)

[Interactive Discussion](#)



References

- Adams, D. D., Hurtgen, M. T., and Sageman, B. B.: Volcanic triggering of a biogeochemical cascade during Oceanic Anoxic Event 2, *Nat. Geosci.*, 3, 201–204, 2010.
- Algeo, T. J., Meyers, P. A., Robinson, R. S., Rowe, H., and Jiang, G. Q.: Icehouse–greenhouse variations in marine denitrification, *Biogeosciences*, 11, 1273–1295, doi:10.5194/bg-11-1273-2014, 2014.
- Asmussen, G. and Strauch, G.: Sulfate reduction in a lake and the groundwater of a former lignite mining area studied by stable sulfur and carbon isotopes, *Water Air Soil Poll.*, 108, 271–284, 1998.
- Bates, A. L., Spiker, E. C., Orem, W. H., and Burnett, W. C.: Speciation and isotopic composition of sulfur in sediments from Jellyfish Lake, Palau, *Chem. Geol.*, 106, 63–76, 1993.
- Bates, A. L., Spiker, E. C., Hatcher, P. G., Stout, S. A., and Weintraub, V. C.: Sulfur geochemistry of organic-rich sediments from Mud Lake, Florida, USA, *Chem. Geol.*, 121, 245–262, 1995.
- Bates, A. L., Spiker, E. C., and Holmes, C. W.: Speciation and isotopic composition of sedimentary sulfur in the Everglades, Florida, USA, *Chem. Geol.*, 146, 155–170, 1998.
- Bekker, A., Holland, H. D., Wang, P. L., Rumble III, D., Stein, H. J., Hannah, J. L., Coetzee, L. L., and Beukes, N. J.: Dating the rise of atmospheric oxygen, *Nature*, 427, 117–120, 2004.
- Berner, R. A.: A model for calcium, magnesium and sulfate in seawater over Phanerozoic time, *Am. J. Sci.*, 304, 438–453, 2004.
- Berner, Z. A., Puchelt, H., Nöltner, T., and Kramar, U.: Pyrite geochemistry in the Toarcian Posidonia Shale of southwest Germany: evidence for contrasting trace-element patterns of diagenetic and syngenetic pyrites, *Sedimentology*, 60, 548–573, 2013.
- Berra, F., Jadoul, F., and Anelli, A.: Environmental control on the end of the Dolomia Principale/Hauptdolomit depositional system in the central Alps: coupling sea-level and climate changes, *Palaeogeogr. Palaeoclimatol. Palaeoecol.*, 290, 138–150, 2010.
- Böttcher, M. E., Voss, M., Schulz-Bull, D., Schneider, R., Leipe, T., and Knöller, K.: Environmental changes in the Pearl River Estuary (China) as reflected by light stable isotopes and organic contaminants, *J. Marine Syst.*, 82, S43–S53, 2010.
- Bottrell, S. H. and Newton, R. J.: Reconstruction of changes in global sulfur cycling from marine sulfate isotopes, *Earth-Sci. Rev.*, 75, 59–83, 2006.
- Bradley, A. S., Leavitt, W. D., and Johnston, D. T.: Revisiting the dissimilatory sulfate reduction pathway, *Geobiology*, 9, 446–457, 2011.

BGD

11, 13187–13250, 2014

Reconstruction of seawater sulfate

T. J. Algeo et al.

[Title Page](#)

[Abstract](#)

[Introduction](#)

[Conclusions](#)

[References](#)

[Tables](#)

[Figures](#)



[Back](#)

[Close](#)

[Full Screen / Esc](#)

[Printer-friendly Version](#)

[Interactive Discussion](#)



Reconstruction of seawater sulfate

T. J. Algeo et al.

[Title Page](#)

[Abstract](#)

[Introduction](#)

[Conclusions](#)

[References](#)

[Tables](#)

[Figures](#)

[◀](#)

[▶](#)

[◀](#)

[▶](#)

[Back](#)

[Close](#)

[Full Screen / Esc](#)

[Printer-friendly Version](#)

[Interactive Discussion](#)



- Brennan, S. T., Lowenstein, T. K., and Horita, J.: Seawater chemistry and the advent of biocalcification, *Geology*, 32, 473–476, 2004.
- Brüchert, V.: Physiological and ecological aspects of sulfur isotope fractionation during bacterial sulfate reduction, in: *Sulfur Biogeochemistry – Past and Present*, edited by: Amend, J. P., Edwards, K. J., and Lyons, T. W., *Geol. Soc. Am. Spec. Pap.*, 379, 1–16, 2004.
- Brüchert, V. and Pratt, L. M.: Contemporaneous early diagenetic formation of organic and inorganic sulfur in estuarine sediments from St. Andrew Bay, Florida, USA, *Geochim. Cosmochim. Ac.*, 60, 2325–2332, 1996.
- Brüchert, V. and Pratt, L. M.: Stable sulfur isotopic evidence fro historical changes of sulfur cycling in estuarine sediments from northern Florida, *Aquat. Geochem.*, 5, 249–268, 1999.
- Brüchert, V., Knoblauch, C., and Jørgensen, B. B.: Microbial controls on the stable sulfur isotope fractionation during bacterial sulfate reduction in Arctic sediments, *Geochim. Cosmochim. Ac.*, 65, 753–766, 2001.
- Brunner, B. and Bernasconi, S. M.: A revised isotope fractionation model for dissimilatory sulfate reduction in sulfate-reducing bacteria, *Geochim. Cosmochim. Ac.*, 69, 4759–4771, 2005.
- Canfield, D. E.: A new model for Proterozoic ocean chemistry, *Nature*, 396, 450–453, 1998.
- Canfield, D. E.: Isotope fractionation by natural populations of sulfate-reducing bacteria, *Geochim. Cosmochim. Ac.*, 65, 1117–1124, 2001.
- Canfield, D. E.: The evolution of the Earth surface sulfur reservoir, *Am. J. Sci.*, 304, 839–861, 2004.
- Canfield, D. E. and Farquhar, J.: Animal evolution, bioturbation, and the sulfate concentration of the oceans, *Proc. Nat. Acad. Sci. (USA)*, 106, 8123–8127, 2009.
- Canfield, D. E. and Raiswell, R.: The evolution of the sulfur cycle, *Am. J. Sci.*, 299, 697–723, 1999.
- Canfield, D. E. and Thamdrup, B. T.: The production of ^{34}S -depleted sulfide during disproportionation of elemental sulfur, *Science*, 266, 1973–1975, 1994.
- Canfield, D. E., Raiswell, R., and Bottrell, S.: The reactivity of sedimentary iron minerals toward sulfide, *Am. J. Sci.*, 292, 659–683, 1992.
- Canfield, D. E., Olesen, C. A., and Cox, R. P.: Temperature and its control of isotope fractionation by a sulfate-reducing bacterium, *Geochim. Cosmochim. Ac.*, 70, 548–561, 2006.
- Canfield, D. E., Poulton, S. W., and Narbonne, G. M.: Late–Neoproterozoic deep-ocean oxygenation and the rise of animal life, *Science*, 315, 92–95, 2007.

- Canfield, D. E., Farquhar, J., and Zerkle, A. L.: High isotope fractionations during sulfate reduction in a low-sulfate euxinic ocean analog, *Geology*, 38, 415–418, 2010.
- Chambers, L. A., Trudinger, P. A., Smith, J. W., and Burns, M. S.: Fractionation of sulfur isotopes by continuous cultures of *Desulfovibrio desulfuricans*, *Can. J. Microbiol.*, 21, 1602–1607, 1975.
- Chanton, J. P. and Lewis, F. G.: Plankton and dissolved inorganic carbon isotopic composition in a river-dominated estuary: apalachicola Bay, Florida, *Estuaries*, 22, 575–583, 1999.
- Chu, X. L., Zhang, T. G., Zhang, Q. R., and Lyons, T. W.: Sulfur and carbon isotope records from 1700 to 800 Ma carbonates of the Jixian section, northern China: Implications for secular isotope variations in Proterozoic seawater and relationships to global supercontinental events, *Geochim. Cosmochim. Ac.*, 71, 4668–4692, 2007.
- Detmers, J., Brüchert, V., Habicht, K. S., and Kuever, J.: Diversity of sulfur isotope fractionations by sulfate-reducing prokaryotes, *Appl. Environ. Microbiol.*, 67, 888–894, 2001.
- DiMichele, W. A. and Hook, R. W.: Paleozoic terrestrial ecosystems, in: *Terrestrial Ecosystems Through Time*, edited by: Behrensmeyer, A. K., Damuth, J. D., DiMichele, W. A., Potts, R., Sues, H.-D., and Wing, S. L., The University of Chicago Press, 205–325, 1992.
- Doi, H., Kikuchi, E., Mizota, C., Satoh, N., Shikano, S., Yurlova, N., Yadrenkina, E., and Zuykova, E.: Carbon, nitrogen, and sulfur isotope changes and hydro-geological processes in a saline lake chain, *Hydrobiologia*, 529, 225–235, 2004.
- Farquhar, J., Peters, M., Johnston, D. T., Strauss, H., Masterson, A., Wiechert, U., and Kaufman, A. J.: Isotopic evidence for Mesoarchaean anoxia and changing atmospheric sulphur chemistry, *Nature*, 449, 706–710, 2007.
- Fike, D. A. and Grotzinger, J. P.: A paired sulfate-pyrite $\delta^{34}\text{S}$ approach to understanding the evolution of the Ediacaran–Cambrian sulfur cycle, *Geochim. Cosmochim. Ac.*, 72, 2636–2648, 2008.
- Fike, D. A., Grotzinger, J. P., Pratt, L. M., and Summons, R. E.: Oxidation of the Ediacaran Ocean, *Nature*, 444, 744–747, 2006.
- Fry, B.: Sources of carbon and sulfur nutrition for consumers in three meromictic lakes of New York State, *Limnol. Oceanogr.*, 31, 79–88, 1986a.
- Fry, B.: Stable sulfur isotopic distributions and sulfate reduction in lake sediments of the Adirondacks Mountains, New York. *Biogeochemistry*, 2, 329–343, 1986b.

Reconstruction of seawater sulfate

T. J. Algeo et al.

[Title Page](#)

[Abstract](#)

[Introduction](#)

[Conclusions](#)

[References](#)

[Tables](#)

[Figures](#)

◀

▶

◀

▶

[Back](#)

[Close](#)

[Full Screen / Esc](#)

[Printer-friendly Version](#)

[Interactive Discussion](#)



Fry, B., Jannasch, H. W., Molyneaux, S. J., Wirsen, C. O., Muramoto, J. A., and King, S.: Stable isotope studies of the carbon, nitrogen and sulfur cycles in the Black Sea and the Cariaco Trench, *Deep-Sea Res.*, A38(Suppl. 2), S1003–S1019, 1991.

5 Fry, B., Giblin, A., and Dornblaser, M.: Stable sulfur isotopic compositions of chromium-reducible sulfur in lake sediments, in: *Geochemical Transformation of Sedimentary Sulfur*, edited by: Vairavamurthy, A. and Schoonens, M. A. A., American Chemical Society, ACS Symposium Series, 612, 397–410, 1995.

Gellatly, A. M. and Lyons, T. W.: Trace sulfate in mid-Proterozoic carbonates and the sulfur isotope record of biospheric evolution, *Geochim. Cosmochim. Ac.*, 69, 3813–3829, 2005.

10 Gill, B. C., Lyons, T. W., and Saltzman, M. R.: Parallel, high-resolution carbon and sulfur isotope records of the evolving Paleozoic marine sulfur reservoir, *Palaeogeogr. Palaeoclimatol. Palaeoecol.*, 256, 156–173, 2007.

Gill, B. C., Lyons, T. W., Young, S. A., Kump, L. R., Knoll, A. H., and Saltzman, M. R.: Geochemical evidence for widespread euxinia in the Later Cambrian ocean, *Nature*, 469, 80–83, 15 2011a.

Gill, B. C., Lyons, T. W., and Jenkyns, H. C.: A global perturbation to the sulfur cycle during the Toarcian Oceanic Anoxic Event, *Earth Planet. Sci. Lett.*, 312, 484–496, 2011b.

Gomes, M. L. and Hurtgen, M. T.: Sulfur isotope systematics of a euxinic, low-sulfate lake: evaluating the importance of the reservoir effect in modern and ancient oceans, *Geology*, 41, 20 663–666, 2013.

Gorlenko, V. M. and Chebotarev, E. N.: Microbiologic processes in meromictic Lake Sakovo, *Microbiology*, 50, 134–139, 1981.

Gorlenko, V. M., Vainstein, B., and Kachalkin, V. I.: Microbiological characteristic of Lake Mogilnoe, *Arch. Hydrobiol.*, 81, 475–492, 1978.

25 Gradstein, F. M., Ogg, J. G., Schmitz, M. D., and Ogg, G. M.: *The Geologic Time Scale 2012*, vol. 2, Elsevier, Amsterdam, 2012.

Guo, Q. J., Strauss, H., Kaufman, A. J., Schröder, S., Gutzmer, J., Wing, B., Baker, M. A., Bekker, A., Jin, Q. S., Kim, S.-T., and Farquhar, J.: Reconstructing Earth's surface oxidation across the Archean-Proterozoic transition, *Geology*, 37, 399–402, 2009.

30 Habicht, K. S. and Canfield, D. E.: Sulphur isotope fractionation in modern microbial mats and the evolution of the sulphur cycle, *Nature*, 382, 342–343, 1996.

Habicht, K. S. and Canfield, D. E.: Sulfur isotope fractionation during bacterial sulfate reduction in organic-rich sediments, *Geochim. Cosmochim. Ac.*, 61, 5351–5361, 1997.

Reconstruction of seawater sulfate

T. J. Algeo et al.

[Title Page](#)

[Abstract](#)

[Introduction](#)

[Conclusions](#)

[References](#)

[Tables](#)

[Figures](#)

◀

▶

◀

▶

[Back](#)

[Close](#)

[Full Screen / Esc](#)

[Printer-friendly Version](#)

[Interactive Discussion](#)



- Habicht, K. S. and Canfield, D. E.: Isotope fractionation by sulfate-reducing natural populations and the isotopic composition of sulfide in marine sediments, *Geology*, 29, 555–558, 2001.
- Habicht, K. S., Gade, M., Thamdrup, B., Berg, P., and Canfield, D. E.: Calibration of sulfate levels in the Archean ocean, *Science*, 298, 2372–2374, 2002.
- 5 Halevy, I., Peters, S. E., and Fischer, W. W.: Sulfate burial constraints on the Phanerozoic sulfur cycle, *Science*, 337, 331–334, 2012.
- Halverson, G. P. and Hurtgen, M. T.: Ediacaran growth of the marine sulfate reservoir, *Earth Planet. Sc. Lett.*, 263, 32–44, 2007.
- 10 Halverson, G. P., Hoffman, P. F., Schrag, D. P., Maloof, A. C., and Rice, A. H. N.: Toward a Neoproterozoic composite carbon-isotope record, *Geol. Soc. Am. Bull.*, 117, 1181–1207, 2005.
- Hartmann, M. and Nielsen, H.: $\delta^{34}\text{S}$ -Werte in rezenten Meeressedimenten und ihre Deutung am Beispiel einiger Sedimentprofile aus der westlichen Ostsee, *Geol. Rundsch.*, 58, 621–655, 1968.
- 15 Holland, H. D.: Volcanic gases, black smokers, and the Great Oxidation Event, *Geochim. Cosmochim. Ac.*, 66, 3811–3826, 2002.
- Holser, W., Maynard, J. B., and Cruikshank, K.: Modelling the natural cycle of sulphur through Phanerozoic time, in: *Evolution of the Global Biogeochemical Sulfur Cycle*, edited by: Brimblecombe, P. and Lein, A. Y., Wiley, New York, 21–56, 1989.
- 20 Horita, J., Zimmermann, H., and Holland, H. D.: Chemical evolution of seawater during the Phanerozoic: implications from the record of marine evaporites, *Geochim. Cosmochim. Ac.*, 66, 3733–3756, 2002.
- Hurtgen, M. T., Arthur, M. A., Suits, N. S., and Kaufman, A. J.: The sulfur isotopic composition of Neoproterozoic seawater sulfate: implications for a snowball Earth?, *Earth Planet. Sc. Lett.*, 203, 413–429, 2002.
- 25 Hurtgen, M. T., Arthur, M. A., and Halverson, G. P.: Neoproterozoic sulfur isotopes, the evolution of microbial sulfur species, and the burial efficiency of sulfide as sedimentary pyrite, *Geology*, 33, 41–44, 2005.
- Hurtgen, M. T., Halverson, G. P., Arthur, M. A., and Hoffman, P. F.: Sulfur cycling in the aftermath of a 635-Ma snowball glaciation: evidence for a syn-glacial sulfidic deep ocean, *Earth Planet. Sc. Lett.*, 245, 551–570, 2006.
- 30 Ivanov, M. V., Rusanov, I. I., Pimenov, N. V., Bairamov, I. T., Yusupov, S. K., Savichev, A. S., Lein, A. Y., and Sapozhnikov, V. V.: Microbial processes of the carbon and sulfur cycles in Lake Mogil'noe, *Microbiology*, 70, 583–593, 2001.

Reconstruction of seawater sulfate

T. J. Algeo et al.

[Title Page](#)[Abstract](#)[Introduction](#)[Conclusions](#)[References](#)[Tables](#)[Figures](#)[Back](#)[Close](#)[Full Screen / Esc](#)[Printer-friendly Version](#)[Interactive Discussion](#)

- Johnston, D. T.: Multiple sulfur isotopes and the evolution of Earth's surface sulfur cycle, *Earth-Sci. Rev.*, 106, 161–183, 2011.
- Johnston, D. T., Wing, B. A., Farquhar, J., Kaufman, A. J., Strauss, H., Lyons, T. W., Kah, L. C., and Canfield, D. E.: Active microbial sulfur disproportionation in the Mesoproterozoic, *Science*, 310, 1477–1479, 2005.
- 5 Johnston, D. T., Farquhar, J., Habicht, K. S., and Canfield, D. E.: Sulphur isotopes and the search for life: strategies for identifying sulphur metabolisms in the rock record and beyond, *Geobiology*, 6, 425–435, 2008.
- 10 Jones, B. A., Facchetti, A., Wasielewski, M. R., and Marks, T. J.: Theory of oxidation-reduction reactions involving electron transfer. 5. Comparison and properties of electrochemical and chemical rate constants, *J. Am. Chem. Soc.*, 129, 15259–15278, 2007.
- Jørgensen, B. B.: Mineralization of organic matter in the sea bed – the role of sulphate reduction, *Nature*, 296, 643–645, 1982.
- 15 Jørgensen, B. B. and Cohen, Y.: Solar Lake (Sinai), 5. The sulfur cycle of the benthic cyanobacterial mats, *Limnol. Oceanogr.*, 22, 657–666, 1977.
- Kah, L. C., Lyons, T. W., and Frank, T. D.: Low marine sulphate and protracted oxygenation of the Proterozoic biosphere, *Nature*, 431, 834–838, 2004.
- 20 Kampschulte, A. and Strauss, H.: The sulfur isotopic evolution of Phanerozoic seawater based on the analysis of structurally substituted sulfate in carbonates, *Chem. Geol.*, 204, 255–286, 2004.
- Kamyshny, Jr., A., Zerkle, A. L., Mansaray, Z. F., Cigleneèki, I., Bura-Nakiæ, E., Farquhar, J., and Ferdelman, T. G.: Biogeochemical sulfur cycling in the water column of a shallow stratified sea-water lake: speciation and quadruple sulfur isotope composition, *Mar. Geol.*, 127, 144–154, 2011.
- 25 Kaplan, I. R.: Stable isotopes of sulfur, nitrogen and deuterium in Recent marine environments, in: *Stable Isotopes in Sedimentary Geology*, edited by: Arthur, M. A., Anderson, T. F., Kaplan, I. R., Veizer, J., and Land, L. S., Society for Sedimentary Geology, Tulsa, Oklahoma, 21–108, 1983.
- Kapan, I. R. and Rittenberg, S. C.: Microbiological fractionation of sulphur isotopes, *J. Gen. Microbiol.*, 34, 195–212, 1964.
- 30 Kaplan, I. R., Emery, K. O., and Rittenberg, S. C.: The distribution and isotopic abundance of sulphur in recent marine sediments off southern California, *Geochim. Cosmochim. Ac.*, 27, 297–331, 1963.

Reconstruction of
seawater sulfate

T. J. Algeo et al.

[Title Page](#)

[Abstract](#)

[Introduction](#)

[Conclusions](#)

[References](#)

[Tables](#)

[Figures](#)

◀

▶

◀

▶

[Back](#)

[Close](#)

[Full Screen / Esc](#)

[Printer-friendly Version](#)

[Interactive Discussion](#)



- Karcz, P.: Relationships between development of organic-rich shallow shelf facies and variation in isotopic composition of pyrite (Middle Triassic, Spitsbergen), Polish Polar Res., 31, 239–254, 2010.
- Karube, Z., Okada, N., and Tayasu, I.: Sulfur stable isotope signature identifies the source of reduced sulfur in benthic communities in macrophyte zones of Lake Biwa, Japan, Limnology, 13, 269–280, 2012.
- Kemp, A. L. W. and Thode, H. G.: The mechanism of the bacterial reduction of sulphate and sulphite from isotope fractionation studies, Geochim. Cosmochim. Ac., 32, 71–91, 1968.
- Kleikemper, J., Schroth, M. H., Bernasconi, S. M., Brunner, B., and Zeyer, J.: Sulfur isotope fractionation during growth of sulfate-reducing bacteria on various carbon sources, Geochim. Cosmochim. Ac., 68, 4891–4904, 2004.
- Ku, T. C. W., Walter, L. M., Coleman, M. L., Blake, R. E., and Martini, A. M.: Coupling between sulfur recycling and syndepositional carbonate dissolution: evidence from oxygen and sulfur isotope composition of pore water sulfate, South Florida Platform, USA, Geochim. Cosmochim. Ac., 63, 2529–2546, 1999.
- Kump, L. R. and Arthur, M. A.: Interpreting carbon-isotope excursions: carbonates and organic matter, Chem. Geol., 161, 181–198, 1999.
- Kurtz, A. C., Kump, L. R., Arthur, M. A., Zachos, J. C., and Paytan, A.: Early Cenozoic decoupling of the global carbon and sulfur cycles, Paleoceanography, 18, PA000908, doi:10.1029/2003PA000908, 2003.
- Leavitt, W. D., Halevy, I., Bradley, A. S., and Johnston, D. T.: Influence of sulfate reduction rates on the Phanerozoic sulfur isotope record, Proc. Nat. Acad. Sci. (USA), 110, 11244–11249, 2013.
- Lee, Y. J. and Lwiza, K.: Interannual variability of temperature and salinity in shallow water: Long Island Sound, New York, J. Geophys. Res., 110, C09022, doi:10.1029/2004JC002507, 2005.
- Lein, A. Y.: Biogeochemistry of the anaerobic diagenesis of Recent Baltic Sea sediments, Environ. Biogeochem., 35, 441–461, 1983.
- Li, C., Love, G. D., Lyons, T. W., Fike, D. A., Sessions, A. L., and Chu, X.: A stratified redox model for the Ediacaran ocean, Science, 328, 80–83, 2010.
- Li, X., Gilhooly III, W. P., Zerkle, A. L., Lyons, T. W., Farquhar, J., Werne, J. P., Varela, R., and Scranton, M. I.: Stable sulfur isotopes in the water column of the Cariaco Basin, Geochim. Cosmochim. Ac., 74, 6764–6778, 2010.

Reconstruction of seawater sulfate

T. J. Algeo et al.

[Title Page](#)[Abstract](#)[Introduction](#)[Conclusions](#)[References](#)[Tables](#)[Figures](#)[◀](#)[▶](#)[◀](#)[▶](#)[Back](#)[Close](#)[Full Screen / Esc](#)[Printer-friendly Version](#)[Interactive Discussion](#)

- Llobet-Brossa, E., Rabus, R., Böttcher, M. E., Könneke, M., Finke, N., Schramm, A., Meyer, R. L., Grötzschel, S., Rosselló-Mora, R., and Amann, R.: Community structure and activity of sulfate-reducing bacteria in an intertidal surface sediment: a multi-method approach, *Aquat. Microbial Ecol.*, 29, 211–226, 2002.
- 5 Lojen, S., Ogrinc, N., Dolenc, T., Vokal, B., Szaran, J., Mihelèiæ, G., and Branica, M.: Nutrient fluxes and sulfur cycling in the organic-rich sediment of Makirina Bay (Central Dalmatia, Croatia), *Sci. Total Environ.*, 327, 265–284, 2004.
- 10 Lowenstein, T. K., Hardie, L. A., Timofeeff, M. N., and Demicco, R. V.: Secular variation in seawater chemistry and the origin of calcium chloride basinal brines, *Geology*, 31, 857–860, 2003.
- Lowenstein, T. K., Timofeeff, M. N., Kovalevych, V. M., and Horita, J.: The major-ion composition of Permian seawater, *Geochim. Cosmochim. Ac.*, 69, 1701–1719, 2005.
- 15 Loyd, S. J., Marenco, P. J., Hagadorn, J. W., Lyons, T. W., Kaufman, A. J., Sour-Tovar, F., and Corsetti, F. A.: Sustained low marine sulfate concentrations from the Neoproterozoic to the Cambrian: insights from carbonates of northwestern Mexico and eastern California, *Earth Planet. Sci. Lett.*, 339–340, 79–94, 2012.
- Loyd, S. J., Marenco, P. J., Hagadorn, J. W., Lyons, T. W., Kaufman, A. J., Sour-Tovar, F., and Corsetti, F. A.: Local $\delta^{34}\text{S}$ variability in ~ 580 Ma carbonates of northwestern Mexico and the Neoproterozoic marine sulfate reservoir, *Precambr. Res.*, 224, 551–569, 2013.
- 20 Luo, G. M., Kump, L. R., Wang, Y., Tong, J., Arthur, M. A., Yang, H., Huang, J., Yin, H., and Xie, S.: Isotopic evidence for an anomalously low oceanic sulphate concentration following end-Permian mass extinction, *Earth Planet. Sci. Lett.*, 300, 101–111, 2010.
- Luo, G. M., Ono, S., Huang, J., Li, C., Algeo, T. J., Zhou, L., and Xie, S.: Return of Archean low oceanic sulfate levels during the earliest Mesoproterozoic, *Precambrian Research*, in review, 25 2014.
- Lyons, T. W.: Sulfur isotopic trends and pathways of iron sulfide formation in upper Holocene sediments of the anoxic Black Sea, *Geochim. Cosmochim. Ac.*, 61, 3367–3382, 1997.
- Lyons, T. W. and Gill, B. C.: Ancient sulfur cycling and oxygenation of the early biosphere, *Elements* 6, 93–99, 2010.
- 30 Mandernack, K. W., Lynch, L., Krouse, H. R., and Morgan, M. D.: Sulfur cycling in wetland peat of the New Jersey Pinelands and its effect on stream water chemistry, *Geochim. Cosmochim. Ac.*, 64, 3949–3964, 2000.

Reconstruction of seawater sulfate

T. J. Algeo et al.

[Title Page](#)[Abstract](#)[Introduction](#)[Conclusions](#)[References](#)[Tables](#)[Figures](#)[◀](#)[▶](#)[◀](#)[▶](#)[Back](#)[Close](#)[Full Screen / Esc](#)[Printer-friendly Version](#)[Interactive Discussion](#)

Reconstruction of seawater sulfate

T. J. Algeo et al.

[Title Page](#)

[Abstract](#)

[Introduction](#)

[Conclusions](#)

[References](#)

[Tables](#)

[Figures](#)

◀

▶

◀

▶

[Back](#)

[Close](#)

[Full Screen / Esc](#)

[Printer-friendly Version](#)

[Interactive Discussion](#)



Mandernack, K. W., Krouse, H. R., and Skei, J. M.: A stable sulfur and oxygen isotopic investigation of sulfur cycling in an anoxic marine basin, Framvaren Fjord, Norway, *Chem. Geol.*, 195, 181–200, 2003.

Matrosov, A. G., Chebotarev, N. Ye., Kudryavtseva, A. J., Zyakun, A. M., and Ivanov, M. V.: Sulfur isotopic composition in freshwater lakes containing H_2S , *Geokhimiya*, 6, 943–7, 1975, and *Geochem. Internat.*, 12, 217–21, 1975.

Mayer, B. and Schwark, L.: A 15 000 year stable isotope record from sediments of Lake Steisslingen, southwest Germany, *Chem. Geol.*, 161, 315–337, 1999.

McArthur, J. M., Donovan, D. T., Thirlwall, M. F., Fouke, B. W., and Mattey, D.: Strontium isotope profile of the early Toarcian (Jurassic) oceanic anoxic event, the duration of ammonite biozones, and belmenite palaeotemperatures, *Earth Planet. Sc. Lett.*, 179, 269–285, 2000.

McFadden, K. A., Huang, J., Chu, X., Jiang, G., Kaufman, A. J., Zhou, C., Yuan, X., and Xiao, S.: Pulsed oxidation and biological evolution in the Ediacaran Doushantuo Formation, *Proc. Nat. Acad. Sci. (USA)*, 105, 3197–3202, 2008.

Millero, F. J.: *Chemical Oceanography*, 3rd edn., CRC Press, Boca Raton, Florida, 2005.

Montañez, I. P., Norris, R. D., Algeo, T. J., Chandler, M. A., Johnson, K. R., Kennedy, M. J., Kent, D. V., Kiehl, J. T., Kump, L. R., Ravelo, A. C., and Turekian, K. K.: *Understanding Earth's Deep Past: Lessons for Our Climate Future*, National Academy of Sciences Press, Washington, DC, 2011.

Nakagawa, M., Ueno, Y., Hattori, S., Umemura, M., Yagi, A., Takai, K., Koba, K., Sasaki, Y., Makabe, A., and Yoshida, N.: Seasonal change in microbial sulfur cycling in monomictic Lake Fukami-ike, Japan, *Limnol. Oceanogr.*, 57, 974–988, 2012.

Nakai, N. and Jensen, M. L.: The kinetic isotope effect in the bacterial reduction and oxidation of sulfur, *Geochim. Cosmochim. Ac.*, 28, 1893–1912, 1964.

Nakai, N., Wada, H., Kiyosu, Y., and Takimoto, M.: Stable isotope studies on the origin and geological history of water and salts in the Lake Vanda area, Antarctica, *Geochem. Jour.*, 9, 7–24, 1975.

Nakano, T., Tayasu, I., Yamada, Y., Hosono, T., Igeta, A., Hyodo, F., Ando, A., Saitoh, Y., Tanaka, T., Wada, E., and Yachi, S.: Effect of agriculture on water quality of Lake Biwa tributaries, Japan. *Sci. Total Environ.*, 389, 132–148, 2008.

Newton, R. J., Reeves, E. P., Kafousia, N., Wignall, P. B., Bottrell, S. H., and Sha, J.-G.: Low marine sulfate concentrations and the isolation of the European epicontinental sea during the Early Jurassic, *Geology*, 39, 7–10, 2011.

- Nriagu, J. O. and Coker, R. D.: Emission of sulfur from Lake Ontario sediments, Limnol. Oceanogr., 21, 485–489, 1976.
- Nriagu, J. O. and Harvey, H. H.: Isotopic variation as an index of sulfur pollution in lakes around Sudbury, Ontario, Nature, 273, 223–224, 1978.
- 5 Nriagu, J. O. and Soon, Y. K.: Distribution and isotopic composition of sulfur in lake sediments of northern Ontario, Geochim. Cosmochim. Ac., 49, 823–834, 1985.
- Oren, A.: Bioenergetic aspects of halophilism, Microbiol. Mol. Biol. Rev., 63, 334–348, 1999.
- Overmann, J., Beatty, J. T., Krouse, H. R., and Hall, K. J.: The sulfur cycle in the chemocline of a meromictic salt lake, Limnol. Oceanogr., 41, 147–156, 1996.
- 10 Owens, J. D., Gill, B. C., Jenkyns, H. C., Bates, S. M., Severmann, S., Kuypers, M. M. M., Woodfine, R. G., and Lyons, T. W.: Sulfur isotopes track the global extent and dynamics of euxinia during Cretaceous Oceanic Anoxic Event 2, Proc. Nat. Acad. Sci. (USA), 110, 18407–18412, 2013.
- 15 Paytan, A., Kastner, M., Campbell, D., and Thiemens, M. H.: Sulfur isotopic composition of Cenozoic seawater sulfate, Science, 282, 1459–1462, 1998.
- Paytan, A., Kastner, M., Campbell, D., and Thiemens, M. H.: Seawater sulfur isotope fluctuations in the Cretaceous, Science, 304, 1663–1665, 2004.
- Peterson, B. J. and Howarth, R. W.: Sulfur, carbon, and nitrogen isotopes used to trace organic matter flow in the salt-march estuaries of Sapelo Island, Georgia. Limnol. Oceanogr., 32, 20 1195–1213, 1987.
- Planavsky, N. J., Bekker, A., Hofmann, A., Owens, J. D., and Lyons, T. W.: Sulfur record of rising and falling marine oxygen and sulfate levels during the Lomagundi event, Proc. Nat. Acad. Sci. (USA), 109, 18300–18305, 2012.
- Price, F. T. and Casagrande, D. J.: Sulfur distribution and isotopic composition in peats from the 25 Okefenokee Swamp, Georgia and the Everglades, Florida, Internat. J. Coal Geol., 17, 1–20, 1991.
- Purdy, K., Hawes, I., Bryant, C. L., Fallackson, A. E., and Nedwell, D. B.: Estimates of sulphate reduction rates in Lake Vanda, Antarctica support the proposed recent history of the lake, Antarct. Sci., 13, 393–399, 2001.
- 30 Rees, C. E.: A steady-state model for sulphur isotope fractionation in bacterial reduction processes, Geochim. Cosmochim. Ac., 27, 1141–1162, 1973.

Reconstruction of seawater sulfate

T. J. Algeo et al.

[Title Page](#)[Abstract](#)[Introduction](#)[Conclusions](#)[References](#)[Tables](#)[Figures](#)[◀](#)[▶](#)[◀](#)[▶](#)[Back](#)[Close](#)[Full Screen / Esc](#)[Printer-friendly Version](#)[Interactive Discussion](#)

Reconstruction of seawater sulfate

T. J. Algeo et al.

- Reuschel, M., Melezhik, V. A., Whitehouse, M. J., Lepland, A., Fallick, A. E., and Strauss, H.: Isotopic evidence for a sizeable seawater sulfate reservoir at 2.1 Ga, *Precambrian Res.*, 192, 78–88, 2012.
- Ries, J. B., Fike, D. A., Pratt, L. M., Lyons, T. W., and Grotzinger, J. P.: Superheavy pyrite ($\delta^{34}\text{S}_{\text{pyr}} > \delta^{34}\text{S}_{\text{CAS}}$) in the terminal Proterozoic Nama Group, southern Namibia: a consequence of low seawater sulfate at the dawn of life, *Geology*, 37, 743–746, 2009.
- Röhl, H.-J., Schmid-Röhl, A., Oschmann, W., Frimmel, A., and Schwark, L.: The Posidonia Shale (Lower Toarcian) of SW-Germany: an oxygen-depleted ecosystem controlled by sea level and palaeoclimate, *Palaeogeogr. Palaeoclimatol. Palaeoecol.* 165, 27–52, 2001.
- Scheiderich, K., Zerkle, A. L., Helz, G. R., Farquhar, J., and Walker, R. J.: Molybdenum isotope, multiple sulfur isotope, and redox-sensitive element behavior in early Pleistocene Mediterranean sapropels, *Chem. Geol.*, 279, 134–144, 2010.
- Schröder, S., Bekker, A., Beukes, N. J., Strauss, H., and Van Niekerk, H. S.: Rise in seawater sulphate concentration associated with the Paleoproterozoic positive carbon isotope excursion: evidence from sulphate evaporites in the ~2.2–2.1 Gyr shallow-marine Lucknow Formation, South Africa, *Terra Nova*, 20, 108–117, 2008.
- Shen, Y. A., Buick, R., and Canfield, D. E.: Isotopic evidence for microbial sulphate reduction in the early Archaean era, *Nature*, 410, 77–81, 2001.
- Sim, M. S., Bosak, T., and Ono, S. H.: Large sulfur isotope fractionation does not require disproportionation, *Science*, 333, 74–78, 2011a.
- Sim, M. S., Ono, S. H., Donovan, K., Templer, S. P., and Bosak, T.: Effect of electron donors on the fractionation of sulfur isotopes by a marine *Desulfovibrio* sp, *Geochim. Cosmochim. Ac.*, 75, 4244–4259, 2011b.
- Song, H. Y., Tong, J., Algeo, T. J., Song, H. J., Qiu, H., Zhu, Y., Tian, L., Bates, S., Lyons, T. W., Luo, G. M., and Kump, L. R.: Early Triassic seawater sulfate drawdown, *Geochim. Cosmochim. Ac.*, 128, 95–113, 2014.
- Sørensen, K. B. and Canfield, D. E.: Annual fluctuations in sulfur isotope fractionation in the water column of a euxinic marine basin, *Geochim. Cosmochim. Ac.*, 68, 503–515, 2004.
- Stam, M. C., Mason, P. R. D., Pallud, C., and Van Cappellen, P.: Sulfate reducing activity and sulfur isotope fractionation by natural microbial communities in sediments of a hypersaline soda lake (Mono Lake, California), *Chem. Geol.*, 278, 23–30, 2010.
- Sternbeck, J. and Sohlenius, G.: Authigenic sulfide and carbonate mineral formation in Holocene sediments of the Baltic Sea, *Chem. Geol.*, 135, 55–73, 1997.

Title Page	Abstract	Introduction
Conclusions	References	
Tables	Figures	
◀	▶	
◀	▶	
Back	Close	
Full Screen / Esc		
	Printer-friendly Version	
	Interactive Discussion	



- Strauss, H.: The isotopic composition of sedimentary sulfur through time, *Palaeogeogr. Palaeoclimatol. Palaeoecol.*, 132, 97–118, 1997.
- Strauss, H.: Geological evolution from isotope proxy signals – sulfur, *Chem. Geol.*, 161, 89–101, 1999.
- 5 Strauss, H.: Sulfur isotopes and the early Archaean sulphur cycle, *Precambr. Res.*, 126, 349–361, 2003.
- Stribling, J. M., Cornwell, J. C., and Currin, C.: Variability of stable sulfur isotopic ratios in *Spartina alterniflora*, *Mar. Ecol. Progr. Ser.*, 166, 73–81, 1998.
- Suits, N. S. and Wilkin, R. T.: Pyrite formation in the water column and sediments of a meromictic lake, *Geology*, 26, 1099–1102, 1998.
- 10 Sweeney, R. E. and Kaplan, I. R.: Stable isotope composition of dissolved sulfate and hydrogen sulfide in the Black Sea, *Mar. Chem.*, 9, 145–152, 1980.
- Valentine, D. L.: Biogeochemistry and microbial ecology of methane oxidation in anoxic environments: a review, *van Leeuwenhoek*, A., 81, 271–282, 2002.
- 15 Wacey, D., McLoughlin, N., Whitehouse, M. J., and Kilburn, M. R.: Two coexisting sulfur metabolisms in a ca. 3400 Ma sandstone, *Geology*, 38, 1115–1118, 2010.
- Werne, J. P., Hollander, D. J., Behrens, A., Schaeffer, P., Albrecht, P., and Damsté, J. S. S.: Timing of early diagenetic sulfurization of organic matter: a precursor-product relationship in Holocene sediments of the anoxic Cariaco Basin, Venezuela, *Geochim. Cosmochim. Ac.*, 64, 1741–1751, 2000.
- 20 Werne, J. P., Lyons, T. W., Hollander, D. J., Formolo, M. J., and Damsté, J. S. S.: Reduced sulfur in euxinic sediments of the Cariaco Basin: sulfur isotope constraints on organic sulfur formation, *Chem. Geol.*, 195, 159–179, 2003.
- Werne, J. P., Lyons, T. W., Hollander, D. J., Schouten, S., Hopmans, E. C., and Damsté, J. S. S.: 25 Investigating pathways of diagenetic organic matter sulfurization using compound-specific sulfur isotope analysis, *Geochim. Cosmochim. Ac.*, 72, 3489–3502, 2008.
- Wijsman, J. W. M., Middelburg, J. J., Herman, P. M. J., Böttcher, M. E., and Heip, C. H. R.: Sulfur and iron speciation in surface sediments along the northwestern margin of the Black Sea, *Mar. Chem.*, 74, 261–278, 2001.
- 30 Wortmann, U. G. and Chernyavsky, B. M.: Effect of evaporite deposition on Early Cretaceous carbon and sulphur cycling, *Nature*, 446, 654–656, 2007.
- Wortmann, U. G. and Paytan, A.: Rapid variability of seawater chemistry over the past 130 million years, *Science*, 337, 334–336, 2012.

Reconstruction of seawater sulfate

T. J. Algeo et al.

[Title Page](#)[Abstract](#)[Introduction](#)[Conclusions](#)[References](#)[Tables](#)[Figures](#)[◀](#)[▶](#)[◀](#)[▶](#)[Back](#)[Close](#)[Full Screen / Esc](#)[Printer-friendly Version](#)[Interactive Discussion](#)

- Wortmann, U. G., Bernasconi, S. M., and Böttcher, M. E.: Hypersulfidic deep biosphere indicates extreme sulfur isotope fractionation during single-step microbial sulfate reduction, *Geology*, 29, 647–650, 2001.
- 5 Wotte, T., Strauss, H., Fugmann, A., and Garbe-Schönberg, D.: Paired $\delta^{34}\text{S}$ data from carbonate-associated sulfate and chromium-reducible sulfur across the traditional Lower-Middle Cambrian boundary of W-Gondwana, *Geochim. Cosmochim. Ac.*, 85, 228–253, 2012.
- 10 Wu, N., Farquhar, J., Strauss, H., Kim, S.-T., and Canfield, D. E.: Evaluating the S-isotope fractionation associated with Phanerozoic pyrite burial, *Geochim. Cosmochim. Ac.*, 74, 2053–2071, 2010.
- Zerkle, A. L., Kamyshny, Jr., A., Kump, L. R., Farquhar, J., Oduro, H., and Arthur, M. A.: Sulfur cycling in a stratified euxinic lake with moderately high sulfate: constraints from quadrupole S isotopes, *Geochim. Cosmochim. Ac.*, 74, 4953–4970, 2010.
- 15 Zhang, S., Jiang, G., Zhang, J., Song, B., Kennedy, M. J., and Christie-Blick, N.: U-Pb sensitive high-resolution ion microprobe ages from the Doushantuo Formation in south China: constraints on late Neoproterozoic glaciations, *Geology*, 33, 473–476, 2005.
- Zhang, S., Jiang, G., and Han, Y.: The age of the Nantuo Formation and Nantuo glaciation in South China, *Terra Nova*, 20, 289–294, 2008.

Reconstruction of
seawater sulfate

T. J. Algeo et al.

[Title Page](#)

[Abstract](#)

[Introduction](#)

[Conclusions](#)

[References](#)

[Tables](#)

[Figures](#)



[Back](#)

[Close](#)

[Full Screen / Esc](#)

[Printer-friendly Version](#)

[Interactive Discussion](#)



Table A1. MSR fractionation data for modern aqueous systems.

Rec.	Site	Env	Type ^a	$\delta^{34}\text{S-sulf}$ (‰)	$\delta^{34}\text{S-py}$ (‰)	$\Delta^{34}\text{S}_{\text{sulf-py}}$ (‰)	± 1 s.d. (‰)	[SO_4^{2-}] (μM)	Reference
1	Linsley Pond, Conn.	FW-O		7.7	-1.0	8.7		45	Nakai and Jensen (1964)
2	Queechy Pond, Conn.	FW-O		5.8	4.6	1.2		48	Nakai and Jensen (1964)
3	Mt. Tom Pond, Conn.	FW-O		6.1	-3.0	9.1		53	Nakai and Jensen (1964)
4	Lake Fukami-ike, Japan	FW-O		-15.0	-22.0	7.0		417	Nakagawa et al. (2012)
5	Lake Ontario	FW-O		6.9	-1.2	8.1		302	Nriagu and Coker (1976)
6	McFarlane Lake, Ontario	FW-O		6.0	-3.0	9.0		250	Nriagu and Soon (1985), Nriagu and Harvey (1978)
7	Kelley Lake, Ontario	FW-O		5.0	-10.0	15.0		5000	Nriagu and Soon (1985)
8	Turkey Lake, Ontario	FW-O		6.0	2.0	4.0		55	Nriagu and Soon (1985)
9	Batchawana Lake, Ontario	FW-O		5.0	2.0	3.0		55	Nriagu and Soon (1985)
10	Okefenokee Swamp, Georgia	FW-O		9.0	6.2	2.8	4.0	521	Price and Casagrande (1991)
11	New Jersey Pinelands-swamp	FW-O		5.0	-8.8	13.8	5.0	400	Manderack et al. (2000)
12	Lake Biwa, Japan	FW-O		2.3	-4.0	6.3	1.5	110	Karube et al. (2012), Nakano et al. (2008)
13	Everglades, Florida (2cores)	FW-O		17.0	10.2	6.8		530	Bates et al. (1998)
14	Mud Lake, Florida (2cores)	FW-O		12.0	4.3	7.7		1000	Bates et al. (1995)
15	Hufeisensee, Germany	FW-E		1.8	-4.1	5.9		1200	Asmussen and Strauch (1998)
16	Lago di Cadagno, Switzerland	FW-E		27.0	-8.0	35.0		2000	Canfield et al. (2010)
17	Steisslingensee, Germany	FW-E		-6.0	-15.0	9.0		490	Mayer and Schwark (1999)
18	McCarrons Lake, MN	FW-E		5.0	-0.1	5.1		302	Gomes and Hurtgen (2013)
19	Aarhus Bay, Denmark	BW-O		21.6	-35.5	56.5	4.5	20747	Johnston et al. (2008)
20	Apalachicola Bay, Florida (EB)	BW-O		12.0	-24.0	36.0	7.0	4149	Chanton and Lewis (1999)
21	Apalachicola Bay, Florida (CP-DB)	BW-O		18.0	-13.5	31.5	7.0	16598	Chanton and Lewis (1999)
22	Monie Bay, Maryland (HWY)	BW-O		22.5	2.4	20.1		300	Stribling et al. (1998)
23	Monie Bay, Maryland (DB2)	BW-O		21.7	-11.1	32.8		6000	Stribling et al. (1998)
24	Monie Bay (BAY)	BW-O		20.8	-22.4	43.2		12448	Stribling et al. (1998)
25	Monie Bay (DB1)	BW-O		21.7	-2.5	24.2		6000	Stribling et al. (1998)
26	Jade Bay, Waddensee, Germany	BW-O		20.5	-22.5	43.0		22500	Llobet-Brossa et al. (2002)
27	Baltic Sea	BW-O				23.5	9.5	8299	Lein (1983)
28	Black Sea	BW-O		21.5	-46.8	68.0	3.0	16000	Johnston et al. (2008)
29	Black Sea	BW-O		18.5	-33.0	51.5	12.0	16000	Wijmans et al. (2001)
30	Logten Lagoon, Denmark	BW-O		26.0	-7.0	33.0		13000	Habicht and Canfield (1997)
31	Everglades, Florida-Little Shark River	BW-O		17.0	-28.0	45.0	5.0	21875	Price and Casagrande (1991)
32	Everglades, Florida-Mud Bay	BW-O		12.0	3.0	9.0	2.0	3125	Price and Casagrande (1991)
33	Sapelo Island, GA	BW-O		21.0	-19.0	40.0		19500	Peterson and Howarth (1987)
34	Lake Chany, Russia	BW-O		29.8	16.6	18.6		2240	Doi et al. (2004)
35	Long Island Sound, Conn.	BW-O		20.5	-12.5	33.0	0.5	7542	Nakai and Jensen (1964)
36	Branford Bay, Conn.	BW-O		20.4	-21.3	41.7	0.5	6802	Nakai and Jensen (1964)
37	Green Lake, NY	BW-E		24.6	-17.7	55.8		13542	Nakai and Jensen (1964), Suits and Wilkin (1998)
38	Fayetteville Green Lake, NY	BW-E		25.9	-30.9	56.8		15000	Fry (1986a, b); Fry et al. (1995)
39	Fayetteville Green Lake, NY	BW-E		32.0	-24.0	57.0		15000	Zerkle et al. (2010)
40	Lake Mogil'noe, Russia	BW-E		30.0	-27.0	57.0		21875	Ivanov et al. (2001)
41	Lake Mogil'noe, Russia	BW-E				39.5	7.5	21875	Gorlenko et al. (1978)
42	Baltic Sea	BW-E				35.0	11.0	9959	Lein (1983)
43	Black Sea	BW-E		19.5	-38.2	57.7	2.5	17500	Wijmans et al. (2001)
44	Black Sea	BW-E				50.5	7.5	17500	Lyons (1997), Wijmans et al. (2001)
45	Black Sea	BW-E				59.0	2.0	17500	Sweeney and Kaplan (1980), Wijmans et al. (2001)
46	Black Sea	BW-E		23.9	-38.0	61.9	4.0	17500	Johnston et al. (2008), Wijmans et al. (2001)
47	Black Sea	BW-E				62.0		17500	Fry et al. (1991), Wijmans et al. (2001)
48	Framvaren Fjord	BW-E		21.0	-22.8	43.8	2.3	18550	Manderack et al. (2003)
49	Gotland Deep, Baltic Sea	BW-E		20.0	-26.0	46.0	6.0	9959	Sternbeck and Sohlenius (1997)
50	Kiel Bay, Baltic Sea	BW-E		20.0	-29.4	49.4	2.0	19565	Hartmann and Nielsen (1968)
51	Maringer Fjord, Norway	BW-E		20.5	-16.0	36.5	6.0	13000	Sørensen and Canfield (2004)
52	Lake Sakovo, Russia	BW-E		14.0	-11.0	27.0		8125	Matrosov et al. (1975), Gorlenko and Chebotarev (1981)
53	Chernyi Kichiyer (Black Kichier)	BW-E				23.0		896	Matrosov et al. (1975)
54	Bol'shoy Kichiyer (Big Kichier)	BW-E				4.1		448	Matrosov et al. (1975)



Discussion Paper | Reconstruction of seawater sulfate

T. J. Algeo et al.

Table A1. Continued.

Rec.	Site	Env Type ^a	$\delta^{34}\text{S-sulf}$ (‰)	$\delta^{34}\text{S-py}$ (‰)	$\Delta^{34}\text{S}_{\text{sulf}, \text{py}}$ (‰)	± 1 s.d. (‰)	[SO_4^{2-}] (μM)	Reference
55	FOAM, Long Island Sound, NY	SW-O	-29.0	49.0	23 237			Canfield et al. (1992), Canfield and Thamdrup (1994), Lee and Lwiza (2005)
56	Black Hole, Long Island Sound	SW-O			41.0		20 747	Canfield and Thamdrup (1994), Lee and Lwiza (2005)
57	NW Control, Long Island Sound, NY	SW-O			58.0		23 237	Canfield and Thamdrup (1994), Lee and Lwiza (2005)
58	Sachem, Long Island Sound, NY	SW-O			34.0		23 237	Canfield and Thamdrup (1994), Lee and Lwiza (2005)
59	Pearl River Delta, China	SW-O	20.5	-20.0	40.5		27 386	Böttcher et al. (2010)
60	San Diego Trough, California Shelf	SW-O	20.4	-28.8	49.2		27 500	Kaplan et al. (1963)
61	Newport Marsh, California	SW-O	20.4	-20.0	40.4		23 571	Kaplan et al. (1963)
62	St Andrew Bay, Florida	SW-O	21.5	-25.8	47.3	4.0	24 897	Brüchert and Pratt (1996)
63	St Andrew Bay, Florida (WB)	SW-O	21.5	-15.5	37.0		28 000	Brüchert and Pratt (1999)
64	St Andrew Bay, Florida (CB)	SW-O	21.5	-19.2	40.7		22 800	Brüchert and Pratt (1999)
76	Makirina Bay, Croatia	HY-O	21.0	-29.0	50.0	2.0	34 025	Lojen et al. (2004)
77	Solar Lake, Egypt	HY-O	23.4	-20.8	44.2	2.0	126 000	Johnston et al. (2008), Jorgensen and Cohen (1977)
78	Solar Lake, Egypt	HY-O	22.0	-17.0	39.0		65 000	Habicht and Canfield (1997), Jorgensen and Cohen (1977)
79	Lake Vanda, Antarctica (deep)	HY-E	46.0	13.9	32.1		55 187	Purdy et al. (2001)
80	Lake Vanda, Antarctica (deep)	HY-E	46.0	10.5	35.5		55 187	Nakai et al. (1975)
81	Mahooney Lake, B.C., Canada	HY-E	27.5	-24.1	51.6	0.5	420 000	Overmann et al. (1996)

Notes:

^a Environment types are hypersaline (HY) (> 40 psu); seawater (SW) (30–40 psu); brackish water (BW) (10–30 psu); and freshwater (FW) (< 10 psu). Depositional environments are further classified as containing oxic (O) or euxinic (E) porewaters.

- [Title Page](#)
- [Abstract](#) | [Introduction](#)
- [Conclusions](#) | [References](#)
- [Tables](#) | [Figures](#)
- [◀](#) | [▶](#)
- [◀](#) | [▶](#)
- [Back](#) | [Close](#)
- [Full Screen / Esc](#)
- [Printer-friendly Version](#)
- [Interactive Discussion](#)



Table A2. Phanerozoic $\delta^{34}\text{S}_{\text{CAS}}$ data (used to generate Table 3).

Paytan et al. (1998)		Kampschulte and Strauss (2004)	
Age (Ma)	$\delta^{34}\text{S}_{\text{CAS}}$ (‰)	Age (Ma)	$\delta^{34}\text{S}_{\text{CAS}}$ (‰)
0.0	20.9	130.0	15.3
0.0	21.0	132.0	15.9
0.0	21.1	133.0	17.0
0.0	21.1	134.0	18.0
0.0	21.3	134.0	17.4
0.0	21.4	134.0	16.2
0.2	20.9	136.0	18.5
0.2	21.1	136.0	15.2
2.2	22.0	136.0	16.7
2.6	22.0	138.0	16.5
3.8	21.9	139.0	16.1
4.8	22.3	140.0	25.0
5.2	21.8	140.0	21.8
5.7	22.1	140.0	14.8
6.0	22.0	142.0	13.3
6.4	22.3	144.0	12.7
6.8	22.3	154.0	16.1
7.8	21.8	157.0	15.3
7.8	22.0	161.0	16.6
8.1	22.3	161.0	15.8
9.3	21.8	164.0	17.5
9.7	22.1	167.0	20.7
10.2	21.9	170.0	18.5
11.4	22.2	173.0	18.1
12.1	22.1	178.0	18.0

Table A2. Continued.

Paytan et al. (1998)		Kampschulte and Strauss (2004)	
Age (Ma)	$\delta^{34}\text{S}_{\text{CAS}}$ (‰)	Age (Ma)	$\delta^{34}\text{S}_{\text{CAS}}$ (‰)
12.6	21.9	184.0	23.6
12.6	22.0	187.0	17.4
12.7	22.0	197.0	14.3
12.7	22.7	208.0	24.4
12.8	22.2	210.0	18.5
12.9	22.7	211.0	18.0
13.4	22.1	214.0	19.0
13.7	22.0	216.0	17.4
14.2	21.7	221.0	19.2
15.1	22.0	225.0	18.5
15.1	22.1	237.0	17.5
15.7	22.4	240.0	20.1
16.3	21.8	242.0	26.4
16.3	22.0	245.0	16.7
17.2	22.1	245.0	15.7
18.1	21.9	246.0	24.5
19.0	21.8	253.0	10.9
20.0	21.6	264.0	12.5
21.0	22.0	289.0	12.5
22.2	22.0	295.0	11.8
23.5	21.9	297.0	12.3
24.1	21.9	298.0	11.0
25.6	21.7	304.0	12.9
26.4	21.4	305.0	13.3
26.4	21.8	306.0	13.8

BGD

11, 13187–13250, 2014

Reconstruction of seawater sulfate

T. J. Algeo et al.

- [Title Page](#)
-
- [Abstract](#) [Introduction](#)
-
- [Conclusions](#) [References](#)
-
- [Tables](#) [Figures](#)
-
- ◀
- ▶
-
- ◀
- ▶
-
- Back
- Close
-
- [Full Screen / Esc](#)
-
- [Printer-friendly Version](#)
-
- [Interactive Discussion](#)
-
- 

Table A2. Continued.

Paytan et al. (1998)		Kampschulte and Strauss (2004)	
Age (Ma)	$\delta^{34}\text{S}_{\text{CAS}}$ (‰)	Age (Ma)	$\delta^{34}\text{S}_{\text{CAS}}$ (‰)
26.4	21.9	306.0	12.6
27.4	21.4	309.0	12.6
28.5	21.2	310.0	13.0
29.0	21.3	311.0	15.4
29.0	21.5	313.0	15.1
29.5	21.7	316.0	15.4
30.0	21.6	316.0	14.5
30.8	21.4	317.0	15.0
31.0	21.7	318.0	16.8
32.6	21.6	318.0	15.0
33.7	22.0	319.0	15.7
33.8	21.8	321.0	17.5
34.2	21.6	321.0	16.7
34.6	21.8	324.0	15.7
35.1	22.4	324.0	14.7
35.1	22.5	324.0	13.5
35.6	22.2	326.0	16.2
36.5	22.5	326.0	15.2
37.5	22.1	327.0	12.1
37.5	22.3	329.0	14.1
39.4	22.2	330.0	15.3
40.5	22.3	331.0	14.0
41.7	22.1	331.0	13.8
43.8	22.4	331.0	12.8
44.5	21.9	332.0	15.0

Reconstruction of seawater sulfate

T. J. Algeo et al.

[Title Page](#)

[Abstract](#)

[Introduction](#)

[Conclusions](#)

[References](#)

[Tables](#)

[Figures](#)

◀

▶

◀

▶

[Back](#)

[Close](#)

[Full Screen / Esc](#)

[Printer-friendly Version](#)

[Interactive Discussion](#)



Table A2. Continued.

Paytan et al. (1998)		Kampschulte and Strauss (2004)	
Age (Ma)	$\delta^{34}\text{S}_{\text{CAS}}$ (‰)	Age (Ma)	$\delta^{34}\text{S}_{\text{CAS}}$ (‰)
44.5	22.0	334.0	14.5
46.0	21.6	334.0	13.7
46.0	21.5	335.0	12.9
48.2	20.3	336.0	15.6
49.7	19.1	337.0	14.5
49.9	19.3	338.0	12.8
50.2	19.1	339.0	13.4
51.2	18.7	343.0	14.6
51.6	18.0	343.0	13.7
51.9	18.1	345.0	15.9
53.6	17.8	346.0	21.2
55.5	17.4	349.0	17.7
56.4	17.7	351.0	18.5
57.0	17.5	353.0	17.6
57.6	18.2	355.0	23.3
57.6	18.3	355.0	21.3
57.9	17.9	360.0	20.6
57.9	18.0	360.0	19.7
59.2	18.1	380.0	22.7
60.7	18.6	380.0	22.0
60.9	19.0	383.0	16.4
61.8	19.1	386.0	17.3
63.9	18.8	391.0	23.3
65.2	19.0	403.0	24.5
65.2	18.9	406.0	28.5

Table A2. Continued.

Paytan et al. (1998)		Kampschulte and Strauss (2004)	
Age (Ma)	$\delta^{34}\text{S}_{\text{CAS}}$ (‰)	Age (Ma)	$\delta^{34}\text{S}_{\text{CAS}}$ (‰)
65.5	19.1	408.0	24.4
66.0	18.8	413.0	26.6
66.8	18.8	422.0	25.8
68.7	18.9	426.0	25.8
68.7	18.9	426.0	24.8
70.0	18.8	426.0	24.5
71.3	19.1	427.0	27.5
73.0	19.2	427.0	23.4
74.2	19.1	432.0	24.3
74.4	19.3	434.0	30.2
75.3	19.4	435.0	28.9
75.6	19.3	436.0	35.6
76.4	19.1	436.0	29.2
78.4	19.0	436.0	28.2
78.8	19.1	436.0	27.6
80.3	19.0	437.0	31.5
82.0	18.9	438.0	26.2
83.0	18.2	439.0	14.5
83.6	18.4	441.0	24.3
83.7	18.4	441.0	24.0
83.9	18.1	443.0	27.0
85.6	18.3	443.0	22.6
88.4	18.3	445.0	31.6
88.4	18.1	445.0	21.8
91.0	18.6	445.0	21.1

[Title Page](#)[Abstract](#)[Introduction](#)[Conclusions](#)[References](#)[Tables](#)[Figures](#)[◀](#)[▶](#)[◀](#)[▶](#)[Back](#)[Close](#)[Full Screen / Esc](#)[Printer-friendly Version](#)[Interactive Discussion](#)

Table A2. Continued.

Paytan et al. (1998)		Kampschulte and Strauss (2004)	
Age (Ma)	$\delta^{34}\text{S}_{\text{CAS}}$ (‰)	Age (Ma)	$\delta^{34}\text{S}_{\text{CAS}}$ (‰)
93.0	18.9	446.0	23.0
93.4	19.1	447.0	32.9
93.5	19.0	454.0	29.3
93.6	18.8	454.0	24.5
93.8	19.0	456.0	27.4
95.0	19.2	461.0	22.9
95.8	19.0	468.0	19.1
97.0	19.1	471.0	26.8
97.0	18.5	472.0	28.7
98.9	17.9	475.0	27.8
98.9	17.8	475.0	25.8
100.0	16.3	477.0	17.6
104.0	15.6	478.0	26.8
104.0	15.6	484.0	29.0
107.0	15.7	484.0	27.6
108.0	15.9	486.0	32.3
109.0	16.1	491.0	30.5
110.0	15.9	510.0	30.8
111.1	16.1	511.0	20.9
111.5	16.3	512.0	36.2
111.9	16.1	512.0	34.5
112.0	16.6	512.0	30.6
112.0	16.0	513.0	29.2
112.0	16.3	514.0	45.4
112.7	16.3	514.0	32.5

[Title Page](#)[Abstract](#)[Introduction](#)[Conclusions](#)[References](#)[Tables](#)[Figures](#)[◀](#)[▶](#)[◀](#)[▶](#)[Back](#)[Close](#)[Full Screen / Esc](#)[Printer-friendly Version](#)[Interactive Discussion](#)

Table A2. Continued.

Paytan et al. (1998)		Kampschulte and Strauss (2004)	
Age (Ma)	$\delta^{34}\text{S}_{\text{CAS}}$ (‰)	Age (Ma)	$\delta^{34}\text{S}_{\text{CAS}}$ (‰)
113.1	15.4	515.0	27.8
116.0	15.5	516.0	50.7
116.0	15.8	516.0	36.4
116.0	15.9	517.0	46.4
116.3	15.3	517.0	40.2
116.5	15.5	518.0	39.1
116.5	15.5	518.0	34.7
119.6	15.5	519.0	30.6
119.8	16.4	521.0	38.5
120.0	17.2	524.0	36.2
120.5	18.7	526.0	39.0
120.7	17.8	527.0	29.7
122.8	19.5	550.0	34.5
122.8	19.2	553.0	31.6
125.0	19.7	556.0	29.4
126.7	20.0	557.0	37.0
129.2	20.1	558.0	30.8
		560.0	38.2
		560.0	34.8
		562.0	37.3
		563.0	34.2

Reconstruction of seawater sulfate

T. J. Algeo et al.

[Title Page](#)[Abstract](#)[Introduction](#)[Conclusions](#)[References](#)[Tables](#)[Figures](#)[◀](#)[▶](#)[◀](#)[▶](#)[Back](#)[Close](#)[Full Screen / Esc](#)[Printer-friendly Version](#)[Interactive Discussion](#)

Reconstruction of seawater sulfate

T. J. Algeo et al.

Title Page

Abstract

Introduction

Conclusion

References

Tables

Figures

Back

Close

Full Screen / Esc

[Printer-friendly Version](#)

Interactive Discussion



Table A3. Phanerozoic seawater sulfate $\delta^{34}\text{S}$ curve.

Age (Ma)	$\delta^{34}\text{S}_{\text{SW}}^{\text{a}}$ (‰) mean	$\delta^{34}\text{S}_{\text{SW}}^{\text{a}}$ (‰) -1 st.dev.	$\delta^{34}\text{S}_{\text{SW}}^{\text{a}}$ (‰) +1 st.dev.	[SO_4^{2-}] mM max	$\Delta^{34}\text{S}_{\text{sulf-py}}^{\text{c}}$ (‰)	[SO_4^{2-}] mM mean	[SO_4^{2-}] mM -1 st.dev.	[SO_4^{2-}] mM +1 st.dev.
0	21.2	20.9	21.5	364	45.8	20.5	11.8	35.7
5	22.0	21.6	22.3	901	45.9	20.6	11.9	35.8
10	22.0	21.7	22.3	2550	46.0	20.7	12.0	36.0
15	22.0	21.7	22.3	1383	46.0	20.7	12.0	36.0
20	21.8	21.4	22.2	1481	45.8	20.5	11.8	35.7
25	21.7	21.3	22.1	942	45.5	20.2	11.6	35.2
30	21.6	21.2	21.9	696	45.6	20.3	11.7	35.3
35	22.0	21.6	22.5	817	45.8	20.5	11.8	35.7
40	22.0	21.3	22.7	244	45.9	20.6	11.9	35.8
45	21.6	20.7	22.4	121	44.4	19.0	10.8	33.4
50	19.2	18.4	20.0	144	42.5	17.1	9.6	30.6
55	18.1	17.2	18.9	297	41.8	16.5	9.1	29.6
60	18.5	17.9	19.2	589	41.8	16.5	9.1	29.6
65	18.9	18.5	19.3	1059	42.1	16.8	9.3	30.0
70	18.9	18.5	19.3	802	42.3	17.0	9.5	30.3
75	19.2	18.9	19.6	504	42.2	16.9	9.4	30.1
80	18.9	18.4	19.4	478	41.4	16.1	8.9	29.0
85	18.4	17.9	18.8	619	41.3	16.0	8.8	28.8
90	18.5	17.9	19.1	274	39.5	14.4	7.8	26.3
95	18.9	18.3	19.4	142	39.4	14.3	7.7	26.2
100	17.3	16.3	18.2	173	40.1	14.9	8.1	27.1
105	16.1	15.2	17.0	449	39.0	14.0	7.5	25.7
110	16.2	15.6	16.7	400	38.6	13.6	7.3	25.1
115	15.9	15.2	16.6	150	38.8	13.8	7.4	25.4
120	17.1	16.0	18.1	101	39.6	14.5	7.8	26.5

Table A3. Continued.

Age (Ma)	$\delta^{34}\text{S}_{\text{SW}}^{\text{a}}$ (‰) mean	$\delta^{34}\text{S}_{\text{SW}}^{\text{a}}$ (‰) –1 st.dev.	$\delta^{34}\text{S}_{\text{SW}}^{\text{a}}$ (‰) +1 st.dev.	[SO ₄ ²⁻] ^b mM max	$\Delta^{34}\text{S}_{\text{sulf-py}}^{\text{c}}$ (‰)	[SO ₄ ²⁻] ^d mM mean	[SO ₄ ²⁻] ^d mM –1 st.dev.	[SO ₄ ²⁻] ^d mM +1 st.dev.
125	19.0	17.7	20.2	124	40.3	15.1	8.2	27.4
130	17.2	15.4	19.0	172	40.5	15.3	8.4	27.7
135	17.1	15.6	18.6	86	42.3	17.0	9.5	30.3
140	18.1	14.9	21.3	60	43.4	18.0	10.2	31.9
145	15.7	12.8	18.7	86	43.0	17.6	9.9	31.3
150	16.7	14.3	19.1	236	42.6	17.2	9.7	30.7
155	16.3	14.9	17.7	283	43.1	17.7	10.0	31.5
160	16.5	15.3	17.8	185	43.8	18.4	10.4	32.5
165	18.0	16.4	19.6	254	43.7	18.3	10.4	32.4
170	18.5	17.2	19.8	442	43.9	18.5	10.5	32.7
175	18.3	16.8	19.7	185	43.7	18.3	10.4	32.4
180	18.9	16.5	21.2	87	45.0	19.7	11.3	34.4
185	19.3	16.6	21.9	68	45.0	19.7	11.3	34.4
190	18.4	15.7	21.1	83	45.2	19.9	11.4	34.7
195	17.5	14.6	20.3	92	45.5	20.2	11.6	35.2
200	17.9	15.0	20.9	75	45.6	20.3	11.7	35.3
205	19.4	16.5	22.3	102	45.9	20.6	11.9	35.8
210	19.3	16.9	21.7	221	46.2	20.9	12.1	36.3
215	18.7	16.7	20.7	335	46.6	21.4	12.4	37.0
220	18.7	16.7	20.7	477	47.3	22.1	12.9	38.1
225	18.7	16.5	20.9	735	48.2	23.1	13.6	39.6
230	18.8	16.0	21.5	284	48.1	23.0	13.6	39.5
235	19.0	16.0	22.1	116	46.9	21.7	12.6	37.4
240	19.8	16.3	23.3	96	46.4	21.1	12.3	36.6
245	19.3	15.5	23.2	88	45.4	20.1	11.5	35.0

Table A3. Continued.

Age (Ma)	$\delta^{34}\text{S}_{\text{SW}}^{\text{a}}$ (‰) mean	$\delta^{34}\text{S}_{\text{SW}}^{\text{a}}$ (‰) –1 st.dev.	$\delta^{34}\text{S}_{\text{SW}}^{\text{a}}$ (‰) +1 st.dev.	[SO ₄ ²⁻] ^b mM max	$\Delta^{34}\text{S}_{\text{sulf-py}}^{\text{c}}$ (‰)	[SO ₄ ²⁻] ^d mM mean	[SO ₄ ²⁻] ^d mM –1 st.dev.	[SO ₄ ²⁻] ^d mM +1 st.dev.
250	17.7	13.3	22.0	75	44.8	19.4	11.1	34.1
255	15.8	11.6	20.1	91	43.7	18.3	10.4	32.4
260	15.4	11.5	19.3	105	41.0	15.7	8.7	28.4
265	14.8	11.3	18.3	109	38.9	13.9	7.5	25.5
270	15.4	11.7	19.0	197	38.4	13.5	7.2	24.9
275	15.4	11.8	19.1	254	37.5	12.7	6.7	23.7
280	15.0	11.6	18.4	165	35.8	11.4	5.9	21.6
285	14.2	11.2	17.2	161	35.0	10.8	5.5	20.6
290	13.6	11.0	16.1	210	34.5	10.4	5.3	20.0
295	13.2	10.9	15.5	234	32.6	9.1	4.5	17.9
300	13.5	11.3	15.6	239	33.0	9.4	4.6	18.3
305	13.8	12.0	15.7	175	30.0	7.5	3.5	15.2
310	14.4	12.6	16.1	126	30.2	7.6	3.6	15.4
315	15.0	13.4	16.7	117	30.3	7.7	3.6	15.5
320	15.3	13.7	16.9	135	30.2	7.6	3.6	15.4
325	15.0	13.3	16.7	196	29.5	7.2	3.3	14.7
330	14.6	13.0	16.3	403	29.0	6.9	3.2	14.2
335	14.7	12.8	16.5	158	29.1	7.0	3.2	14.3
340	15.1	12.8	17.4	74	29.1	7.0	3.2	14.3
345	16.4	13.7	19.1	59	29.4	7.1	3.3	14.6
350	17.8	15.0	20.6	50	27.5	6.1	2.7	12.8
355	19.1	16.2	21.9	74	28.7	6.7	3.1	13.9
360	19.4	16.6	22.2	196	29.7	7.3	3.4	14.9
365	19.4	16.1	22.6	287	30.2	7.6	3.6	15.4
370	19.7	16.1	23.4	158	30.3	7.7	3.6	15.5

Reconstruction of seawater sulfate

T. J. Algeo et al.

- [Title Page](#) |
 [Discussion Paper](#) |
 [Abstract](#) |
 [Introduction](#) |
 [Conclusions](#) |
 [References](#) |
 [Tables](#) |
 [Figures](#) |
 [◀](#) |
 [▶](#) |
 [◀](#) |
 [▶](#) |
 [Back](#) |
 [Close](#) |
 [Full Screen / Esc](#) |
 [Printer-friendly Version](#) |
 [Interactive Discussion](#)



Table A3. Continued.

Age (Ma)	$\delta^{34}\text{S}_{\text{SW}}^{\text{a}}$ (‰) mean	$\delta^{34}\text{S}_{\text{SW}}^{\text{a}}$ (‰) –1 st.dev.	$\delta^{34}\text{S}_{\text{SW}}^{\text{a}}$ (‰) +1 st.dev.	[SO_4^{2-}] ^b mM max	$\Delta^{34}\text{S}_{\text{sulf-py}}^{\text{c}}$ (‰)	[SO_4^{2-}] ^d mM mean	[SO_4^{2-}] ^d mM –1 st.dev.	[SO_4^{2-}] ^d mM +1 st.dev.
375	20.3	16.8	23.9	69	30.3	7.7	3.6	15.5
380	20.5	17.3	23.7	38	30.4	7.7	3.6	15.6
385	20.0	16.6	23.4	38	29.2	7.0	3.2	14.4
390	21.3	17.7	24.9	74	29.0	6.9	3.2	14.2
395	22.7	18.8	26.5	84	28.7	6.7	3.1	13.9
400	24.1	20.4	27.7	67	29.4	7.1	3.3	14.6
405	25.1	22.0	28.3	92	29.5	7.2	3.3	14.7
410	25.3	22.2	28.4	177	29.6	7.2	3.4	14.8
415	25.5	22.4	28.7	310	31.5	8.4	4.0	16.7
420	25.6	22.6	28.6	276	32.0	8.7	4.2	17.3
425	25.7	22.9	28.5	108	32.3	8.9	4.3	17.6
430	26.4	23.1	29.7	45	32.8	9.3	4.5	18.1
435	27.1	23.3	31.0	36	33.3	9.6	4.8	18.7
440	25.9	21.8	30.0	54	31.9	8.7	4.2	17.1
445	25.7	21.8	29.6	106	31.1	8.2	3.9	16.3
450	26.2	22.3	30.1	104	30.0	7.5	3.5	15.2
455	26.3	22.8	29.7	79	28.4	6.6	3.0	13.6
460	25.6	21.9	29.3	93	27.9	6.3	2.8	13.2
465	25.1	21.1	29.2	105	26.8	5.7	2.5	12.2
470	25.6	21.7	29.5	161	29.0	6.9	3.2	14.2
475	25.9	22.1	29.8	113	28.8	6.8	3.1	14.0
480	26.7	22.5	30.9	63	29.4	7.1	3.3	14.6
485	28.5	24.6	32.5	98	30.5	7.8	3.7	15.7
490	29.6	25.2	33.9	207	31.1	8.2	3.9	16.3
495	30.5	25.2	35.7	154	31.4	8.3	4.0	16.6

Table A3. Continued.

Age (Ma)	$\delta^{34}\text{S}_{\text{SW}}^{\text{a}}$ (‰) mean	$\delta^{34}\text{S}_{\text{SW}}^{\text{a}}$ (‰) –1 st.dev.	$\delta^{34}\text{S}_{\text{SW}}^{\text{a}}$ (‰) +1 st.dev.	[SO_4^{2-}] ^b mM max	$\Delta^{34}\text{S}_{\text{sulf-py}}^{\text{c}}$ (‰)	[SO_4^{2-}] ^d mM mean	[SO_4^{2-}] ^d mM –1 st.dev.	[SO_4^{2-}] ^d mM +1 st.dev.
500	31.8	25.8	37.8	113	31.2	8.2	3.9	16.4
505	32.8	26.7	38.8	49	31.4	8.3	4.0	16.6
510	33.5	27.4	39.5	37	31.0	8.1	3.9	16.2
515	35.7	29.6	41.8	75	28.6	6.7	3.0	13.8
520	36.3	30.8	41.8	199	28.9	6.8	3.1	14.1
525	35.5	30.5	40.5	115	29.6	7.2	3.4	14.8
530	34.7	29.6	39.8	186	29.9	7.4	3.5	15.1
535	34.2	28.9	39.5	449	30.4	7.7	3.6	15.6
540	33.7	28.7	38.8	281	22.1	3.6	1.4	8.5
545	33.5	29.2	37.8	109	21.3	3.3	1.2	7.9
550	33.4	30.0	36.7	38	18.9	2.5	0.8	6.3
555	33.4	30.2	36.6	28	17.4	2.0	0.6	5.5
560	34.4	31.4	37.4	39	16.7	1.9	0.5	5.1
565	34.6	31.5	37.7	153	15.8	1.6	0.4	4.6

Notes:

^a $\delta^{34}\text{S}_{\text{SW}}$ values for LOWESS curve calculated from data in Table 2; shown in Fig. 3a.^b [SO_4^{2-}](max) calculated from $\delta^{34}\text{S}_{\text{SW}}$ in col B using Eqs. (1)–(3); shown in Fig. 4.^c $\Delta^{34}\text{S}_{\text{sulf-py}}$ values from Fig. 3 of Wu et al. (2010), GCA 74:2053–2071; shown in Fig. 3c.^d [SO_4^{2-}] values calculated from MSR fractionation relationship (Eqs. 5–7); shown in Fig. 4.

Reconstruction of seawater sulfate

T. J. Algeo et al.

Title Page

Abstract

Introduction

Conclusions

References

Tables

Figures

◀

▶

◀

▶

Back

Close

Full Screen / Esc

Printer-friendly Version

Interactive Discussion



Reconstruction of
seawater sulfate

T. J. Algeo et al.

Table A4. Analysis of high-frequency seawater sulfate variation.

Rec.	Unit	Location	System	Age (Ma)	n	$\Delta^{34}\text{S}_{\text{surf-py}}$ (‰)	$\delta^{34}\text{S}_{\text{CASshift}}$	$\partial\delta^{34}\text{S}_{\text{CAS}}/\partial t$ (max) (‰ Myr ⁻¹)
Neoproterozoic units (Fig. 6)								
a	Iwr Doushantuo Fm	China	up Proterozoic	636–570	40	11.6 (±6.3)	38 to 24‰ over 636–633 Ma	5 (±2X)
b	Brachina Fm/Wilpene Grp	Namibia	up Proterozoic	636–620	2	31 (±5)	18 to 42‰ over 636–620 Ma	1.5 (±2X)
c	Maieberg Fm/Otavi Grp	Namibia	up Proterozoic	636–620	5	11.2 (±15.2)	31 to 14‰ over ~ 636–635 Ma	17 (±3X)
d	Sonora succession	Sonora	Iwr Ediacaran	600–580	11	7.4 (±4.2)	17 to 29‰ over ~ 2 Myr	6 (±3)
e	Wonoka Fm/Wilpene Grp	Namibia	up Proterozoic	585–581	4	39 (±6)	22 to 18‰ over 585–581 Ma	1.0 (±3X)
f	Sonora succession	Sonora	up Ediacaran	580–542	8	14.6 (±7.0)	33 to 18‰ over ~ 4 Myr	4 (±2)
g	up Doushantuo Fm	China	up Proterozoic	570–551	17	23.9 (±9.3)	35 to 11‰ over 568–551	1.3 (±2X)
h	Zarls Fm/Nama Grp	Namibia	up Proterozoic	555–542	18	5.8 (±3.4)	30 to 70‰ at 549–548 Ma	40 (±2X)
j	upper Huqf Supergroup	Oman	up Proterozoic–Cambrian	> 580–540	70	30.0 (±5.7)	23 to 43‰ at 548–547 Ma	20 (±2X)
k	Death Valley succession	Death Valley	Proterozoic–Cambrian	544–542	30	11.3 (±7.1)	24 to 37‰ over ~ 1.2 Myr	11 (±6)
Paleozoic units (Fig. 7)								
m	Sonora succession	Sonora	Cambrian/Terreneuvian	542–520	6	15.7 (±6.5)	34 to 8‰ in ~ 4 Myr	7 (±4)
n	Sonora succession	Sonora	Cambrian/Series 2–3	520–505	3	11.3 (±8.5)	8 to 38‰ in ~ 1.4 Myr	22 (±11)
n'	Death Valley succession	Death Valley	Cambrian/Series 2–3	520–505	1	11	31 to 14‰ in ~ 0.8 Myr	23 (±11)
p	Lancara Fm–Genestosa	Spain	Lower–Middle Cambrian	520–505	19	16.1 (±3.6)	18 to 27‰ in ~ 1 Myr	9 (±3X)
p'	Lancara Fm–Cremenes	France	Lower–Middle Cambrian	520–505	36	10.8 (±4.4)	22 to 29‰ in ~ 0.3 Myr	20 (±3X)
q	Spice excursion	Australia	Upper Cambrian	499–494	11	26.0 (±9.8)	63 to 35‰ at 495.4–494.0 Ma	20 (±1.5X) ^b
q'	Spice excursion	Missouri, USA	Upper Cambrian	499–494	8	28.8 (±10.1)	38 to 27‰ at 496.2–495.2 Ma	11 (±1.5X) ^b
q''	Spice excursion	Nevada, USA	Upper Cambrian	499–494	2	2.1 (±4.9)	46 to 33‰ at 494.9–493.3 Ma	8 (±1.5X) ^b
Meso–Cenozoic units (Fig. 8)								
r	Nanpanjiang Basin carb	China	Lower Triassic	252–250	143	36 (±4)	25 to 33‰ over ~ 0.3 Myr	25 (±2X)
s	Bravaisberget Fm	Spitsbergen	Middle Triassic	245–238	40	15.1 (±5.6)	14 to 22‰ over 1.2 Myr ^d	4 (±2X)
t	Toarcian succession	England	Lower Jurassic	183–178 ^c	~ 60	51 (±6) ^e	16.5 to 22.5‰ in 300 kyr	20 (±4)
t'	Toarcian succession	England	Lower Jurassic	183–178 ^c	55	51 (±6) ^e	16 to 22‰ in 300 kyr	20 (±4)
t'	Toarcian succession	Tibet	Lower Jurassic	183–178 ^c	25	51 (±6) ^e	19 to 37‰ in 300 kyr (?)	60 (±30) (?)
v	Early Cretaceous	South Atlantic	Lower Cretaceous	120–118	~ 100	46 (±4) ^f	15.5 to 20.0‰ in 1.2 Myr	12–16
w	Cenomanian–Turonian	Colorado, USA	Middle Cretaceous	94–93	22	46 (±4) ^f	12 to 19‰ in 400 kyr	15–20
w'	Cenomanian–Turonian	England	Middle Cretaceous	94–93	~ 50	45 (±7) ^f	18 to 22‰ in 600 kyr	6–7
w''	Cenomanian–Turonian	Italy	Middle Cretaceous	94–93	~ 80	47 (±7) ^f	20 to 24‰ in 600 kyr	6–7
z	Sapropel	Mediterranean	Pleistocene	1.8–1.4	11	+60.4 (±4.8)	N/A	< 0.5 ^g



Title Page

Abstract

Introduction

Conclusions

References

Tables

Figures



Full Screen / Esc

Printer-friendly Version

Interactive Discussion

Table A4. Continued.

Rec.	Ocean model ^a	[SO ₄ ²⁻] _{sw} (Rate method) (mM)	[SO ₄ ²⁻] _{sw} (MSR-trend method) (mM)
Neoproterozoic units (Fig. 6)			
a	O	0.5–6	0.1–3
b	O	8–52	5–16
c	O	< 0.1–3	< 0.1–7
d	A	0.2–1.2	< 0.1–1.0
e	A	25–> 100	24–70
f	A	3–22	0.5–11
g	A	13–100	3–35
h	A	0.1–1.0	< 0.1–1.6
j	A	1.5–8	12–45
k	A	0.3–4	0.1–8
Paleozoic units (Fig. 7)			
m	A	2–18	0.8–14
n	A	0.2–4	< 0.1–9
n'	A	0.7–3.5	1.2–2.8
p	A	1.2–14	2–8
p'	A	0.3–5	0.3–6
q	A	1.2–6	4–40
q'	A	2–12	5–13
q''	A	0.1–2.5	2–6
Meso–Cenozoic units (Fig. 8)			
r	O	0.5–2.5	8–20
s	A	3–22	1–10
t	O	1.5–3	18–50
t'	O	1.5–3	18–50
t'	O	0.5–2	18–50
v	O	2.5–4	15–30
w	O	1.5–3	15–30
w'	O	5–8	12–40
w''	O	5–8	12–40
z	O	60–120	n/a

Notes:

- ^a Compared to the oxic (O) ocean model, the anoxic (A) model yields seawater sulfate concentrations that are larger by a factor of 2.4x.
- ^b Rates also given in Table 5 of Gill et al. (2007).
- ^c Age control from McArthur et al. (2000).
- ^d $\delta^{34}\text{S}_{\text{CAS}}/\delta t(\text{max})$ estimated from Song et al. (2014).
- ^e CAS $\delta^{34}\text{S}$ values are 16.4‰ and 37‰ for the *tenunicostatum* and *falciferum* zones, respectively. Pyrite $\delta^{34}\text{S}$ values are $-37 \pm 5\%$ and $-12 \pm 3\%$ for the same zones, respectively (from Berner et al., 2013).
- ^f Based on Cretaceous pyrite $\delta^{34}\text{S}$ data of Strauss (1997, 1999).
- ^g Based on Cenozoic sulfate $\delta^{34}\text{S}$ data of Paytan et al. (1998).

Reconstruction of seawater sulfate

T. J. Algeo et al.

Title Page

Abstract

Introduction

Conclusions

References

Tables

Figures

◀

▶

◀

▶

Back

Close

Full Screen / Esc

Printer-friendly Version

Interactive Discussion



Reconstruction of seawater sulfate

T. J. Algeo et al.

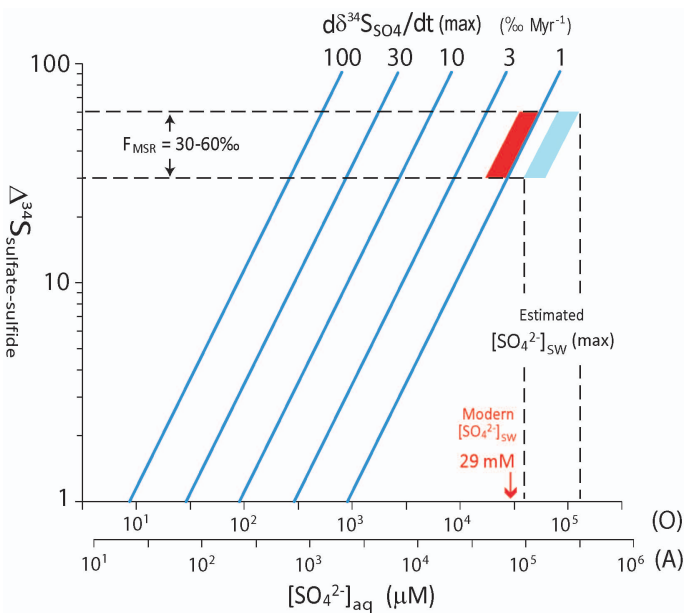


Figure 1. Aqueous sulfate concentrations ($[SO_4^{2-}]_{aq}$) vs. S-isotopic fractionation between cogenetic sulfate and sulfide ($\Delta^{34}S_{\text{sulfate-sulfide}}$). The diagonal blue lines represent maximum rates of change in sulfate $\delta^{34}\text{S}$ (i.e., $\partial\delta^{34}S_{SO_4}/\partial t(\text{max})$). For paleomarine systems, maximum seawater sulfate concentrations ($[SO_4^{2-}]_{sw}$) can be estimated from the abscissa based on measured values of $\Delta^{34}S_{\text{CAS-PY}}$ and $\partial\delta^{34}S_{\text{CAS}}/\partial t(\text{max})$. The two scales on the abscissa represent $[SO_4^{2-}]_{sw}$ in oxic (O) and anoxic (A) oceans, in which pyrite burial fluxes are equal to $4 \times 10^{13} \text{ g yr}^{-1}$ and $10 \times 10^{13} \text{ g yr}^{-1}$ (i.e., 40 % and 100 % of the total S sink flux), respectively. The typical range of $\Delta^{34}S_{\text{sulfate-sulfide}}$ due to MSR in modern seawater is 30–60 ‰ (Habicht and Canfield, 1997). The maximum rate of seawater sulfate $\delta^{34}\text{S}$ variation during the Cenozoic is $\sim 0.5\text{‰ Myr}^{-1}$ (Paytan et al., 1998), yielding estimates of $\sim 40\text{--}110 \text{ mM}$ for $[SO_4^{2-}]_{sw}$ through projection to the abscissa (dashed lines). These estimates exceed actual modern seawater $[SO_4^{2-}]$, which is $\sim 29 \text{ mM}$ (Millero, 2005) because the observed maximum rate of $\partial\delta^{34}S_{SO_4}/\partial t$ (light blue parallelogram) is less than the theoretical possible maximum rate ($\sim 1\text{--}2\text{‰ Myr}^{-1}$; red parallelogram).

Title Page	Abstract	Introduction
Conclusions	References	
Tables	Figures	
◀	▶	
◀	▶	
Back	Close	
Full Screen / Esc		
Printer-friendly Version		
Interactive Discussion		



Reconstruction of seawater sulfate

T. J. Algeo et al.

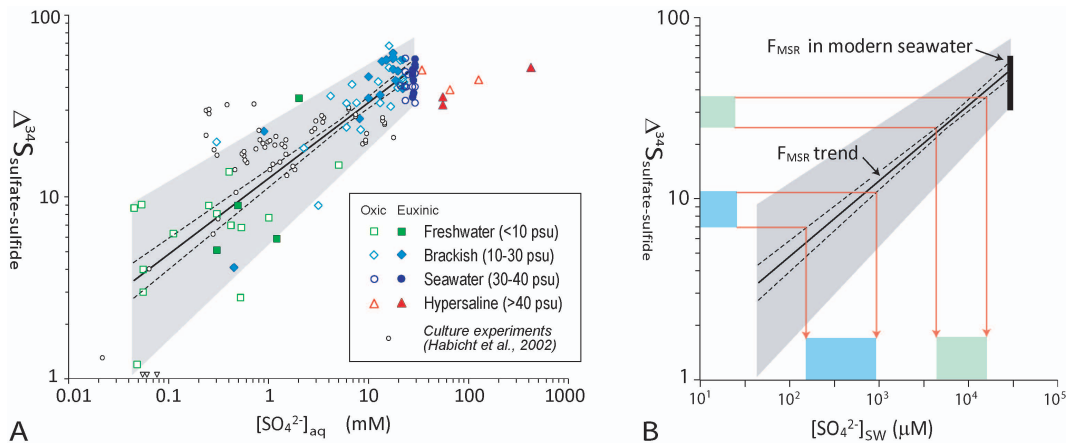


Figure 2. Aqueous sulfate concentration ($[\text{SO}_4^{2-}]_{\text{aq}}$) vs. S-isotopic fractionation between aqueous sulfate and aqueous or sedimentary sulfide ($\Delta^{34}\text{S}_{\text{sulfate-sulfide}}$). **(A)** Data from 81 modern aqueous systems (Table A1) yield a linear regression (solid line; $y = 0.42x - 0.15$ in log units) with $r^2 = 0.80$ and a narrow regression-line uncertainty (dashed lines). F_{MSR} is thus a process with an order of reaction (n) of 0.42 and a rate constant (k) of -0.15 (cf. Jones et al., 2007). The gray field encloses most of the data from Table A1 and highlights the overall trend. Separate analysis by redox environment yielded statistically indistinguishable trends for oxic ($y = 0.48x - 0.26$, $r^2 = 0.77$, $n = 44$) and euxinic settings ($y = 0.40x - 0.08$, $r^2 = 0.80$, $n = 31$). The Habicht et al. (2002) dataset of 60 experimental determinations of MSR is shown for comparison; these data have been converted from their original log-linear to log-log format, and data points that are off scale (with $\Delta^{34}\text{S}_{\text{sulfate-sulfide}} < 1\%$) are shown by triangles on the abscissa. Neither the 6 hypersaline environments in our dataset (red symbols) nor the Habicht et al. data (small open circles) were included in the regression analysis. **(B)** Use of the MSR trend to estimate ancient seawater $[\text{SO}_4^{2-}]_{\text{aq}}$. Measured values of $\Delta^{34}\text{S}_{\text{sulfate-sulfide}}$ are projected from the ordinal scale to the MSR trend and then to the abscissa. Note that uncertainty in the slope of the MSR trend is taken into consideration by projection to the upper uncertainty limit for $\Delta^{34}\text{S}_{\text{sulfate-sulfide}}$ maxima and to the lower uncertainty limit for $\Delta^{34}\text{S}_{\text{sulfate-sulfide}}$ minima. The vertical black bar at $[\text{SO}_4^{2-}]_{\text{aq}} = 4.45$ (i.e., the modern seawater sulfate concentration of 29 mM) represents the range of F_{MSR} variation among modern marine microbial communities.

- [Title Page](#)
- [Abstract](#) [Introduction](#)
- [Conclusions](#) [References](#)
- [Tables](#) [Figures](#)
- [◀](#) [▶](#)
- [◀](#) [▶](#)
- [Back](#) [Close](#)
- [Full Screen / Esc](#)
- [Printer-friendly Version](#)
- [Interactive Discussion](#)



Reconstruction of seawater sulfate

T. J. Algeo et al.

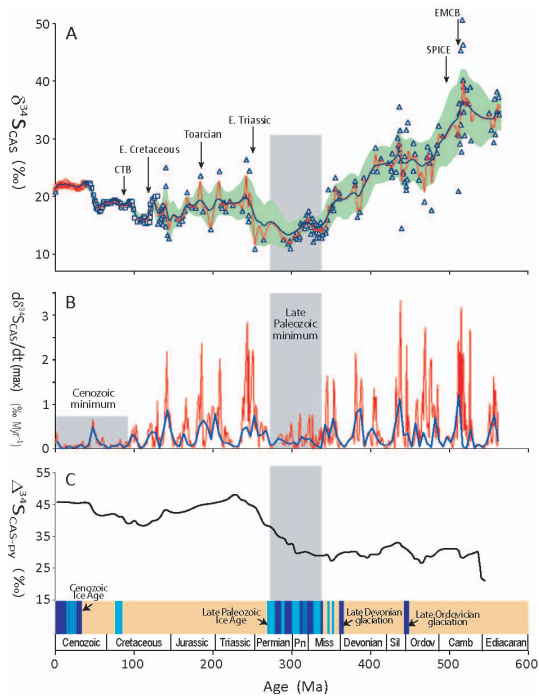


Figure 3. (A) Phanerozoic seawater sulfate $\delta^{34}\text{S}$. Data sources: Cenozoic (Paytan et al., 1998; red circles), Cretaceous (Paytan et al., 2004; black squares), and pre-Cretaceous (Kampschulte and Strauss, 2004; blue triangles; Table A2). Average secular variation in $\delta^{34}\text{S}_{\text{SO}_4-\text{sw}}$ is shown by LOWESS means (blue line for calculations at 5 Myr steps; red line for 1 Myr steps) and a standard deviation range (green field for 5 Myr steps; Table A3). Pre-Cretaceous and Cretaceous–Cenozoic estimates have uncertainties of $\pm 2\text{--}7\text{\textperthousand}$ and $\pm < 1\text{\textperthousand}$, respectively. The labels represent four short (< 2 Myr) intervals of known high-frequency $\partial \delta^{34}\text{S}_{\text{SO}_4}/\partial t$ variation (EMCB = Early–Middle Cambrian boundary; SPICE = Steptoean positive carbon isotope excursion; see text for discussion; CTB = Cenomanian–Turonian boundary). (B) Rate of seawater $\delta^{34}\text{S}$ variation ($\partial \delta^{34}\text{S}_{\text{SO}_4}/\partial t$), as calculated from the seawater sulfate $\delta^{34}\text{S}$ LOWESS curves. The maximum Phanerozoic $\partial \delta^{34}\text{S}_{\text{SO}_4}/\partial t$ is $< 4\text{\textperthousand Myr}^{-1}$, although rates of 10 to $> 50\text{\textperthousand Myr}^{-1}$ have been reported from some high-resolution CAS studies. (C) $\Delta^{34}\text{S}_{\text{CAS-PY}}$ for Phanerozoic marine sediments. Data from Fig. 3 of Wu et al. (2010). The continental glaciation record is adapted from Montañez et al. (2011); all ages were converted to the Gradstein et al. (2012) timescale.

Reconstruction of seawater sulfate

T. J. Algeo et al.

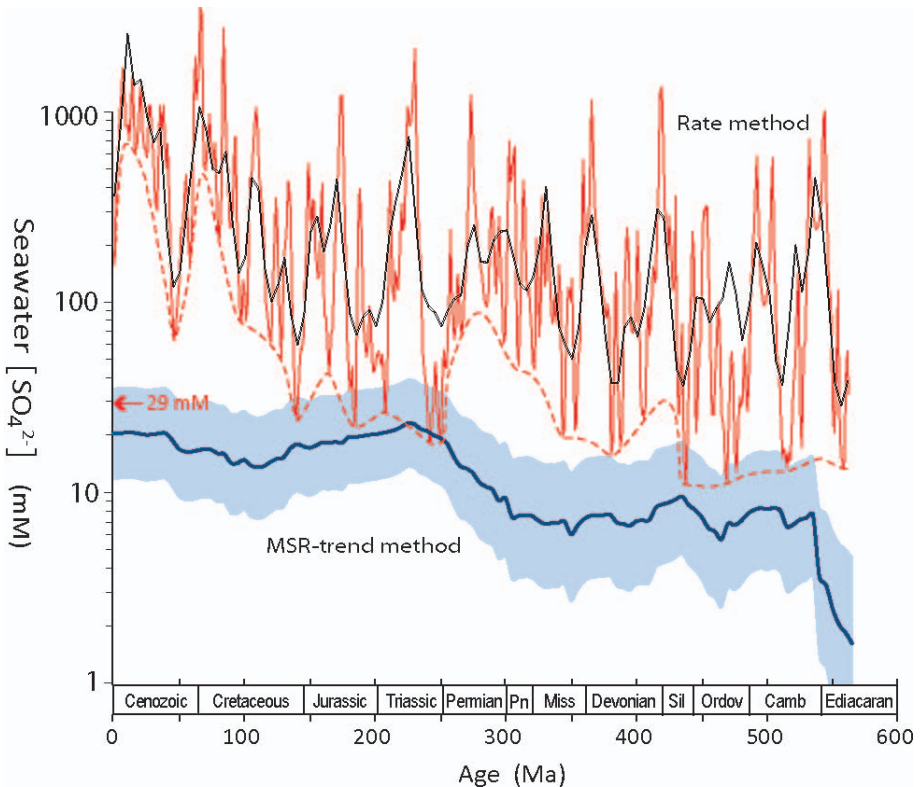


Figure 4. Phanerozoic seawater $[\text{SO}_4^{2-}]$ (Table A3). The MSR-trend method (Eqs. 6–8) yields an estimate of mean $[\text{SO}_4^{2-}]_{\text{SW}}$ (blue curve; bracketed by a ± 1 s.d. band). The rate method (Eqs. 3 and 4) yields the maximum possible $[\text{SO}_4^{2-}]_{\text{SW}}$; the black and red curves show maximum values based on the low- and high-frequency Phanerozoic $\delta^{34}\text{S}_{\text{CAS}}$ records, respectively (Fig. 3), and the dashed red line represents the lower envelope of the high-frequency curve. The modern seawater $[\text{SO}_4^{2-}]$ of $\sim 29 \text{ mM}$ is shown by the red arrow.

Reconstruction of seawater sulfate

T. J. Algeo et al.

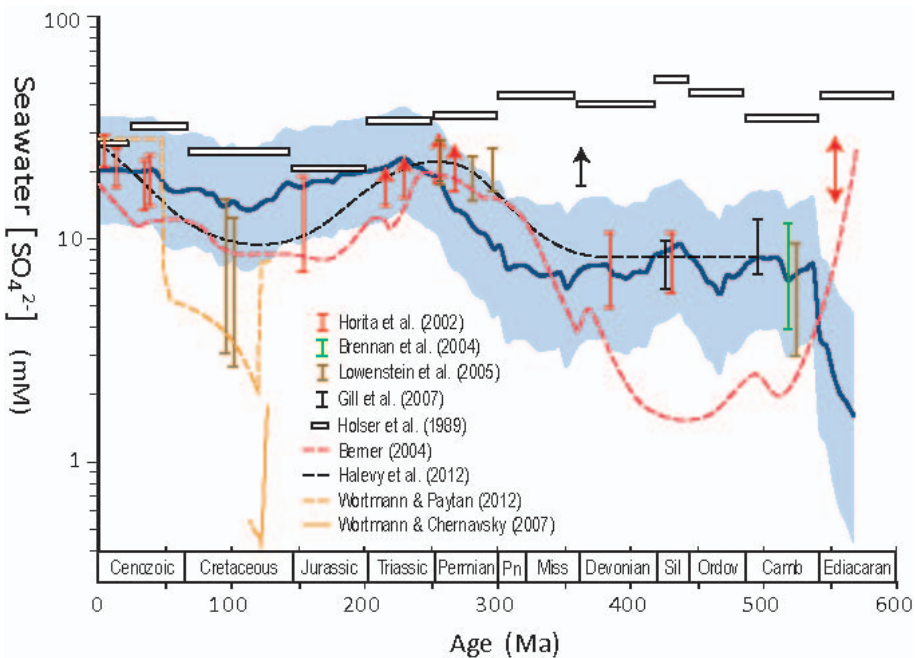


Figure 5. Comparison of Phanerozoic seawater sulfate $[\text{SO}_4^{2-}]$ records. The mean trend of the present study is shown by a heavy blue line, with the $\pm 1\sigma$ uncertainty range shown as a blue band. Estimates are based either on fluid-inclusion studies (Horita et al., 2002; Brennan et al., 2004; Lowenstein et al., 2005) or C-S-cycle modeling (Holser et al., 1989; Berner, 2004; Gill et al., 2007; Wortmann and Chernyavsky, 2007; Wortmann and Paytan, 2012; Halevy et al., 2012). Arrows indicate unconstrained minimum or maximum values.

Title Page	Abstract	Introduction
Conclusions	References	
Tables	Figures	
◀	▶	
◀	▶	
Back	Close	
Full Screen / Esc		
Printer-friendly Version		
Interactive Discussion		



Reconstruction of seawater sulfate

T. J. Algeo et al.

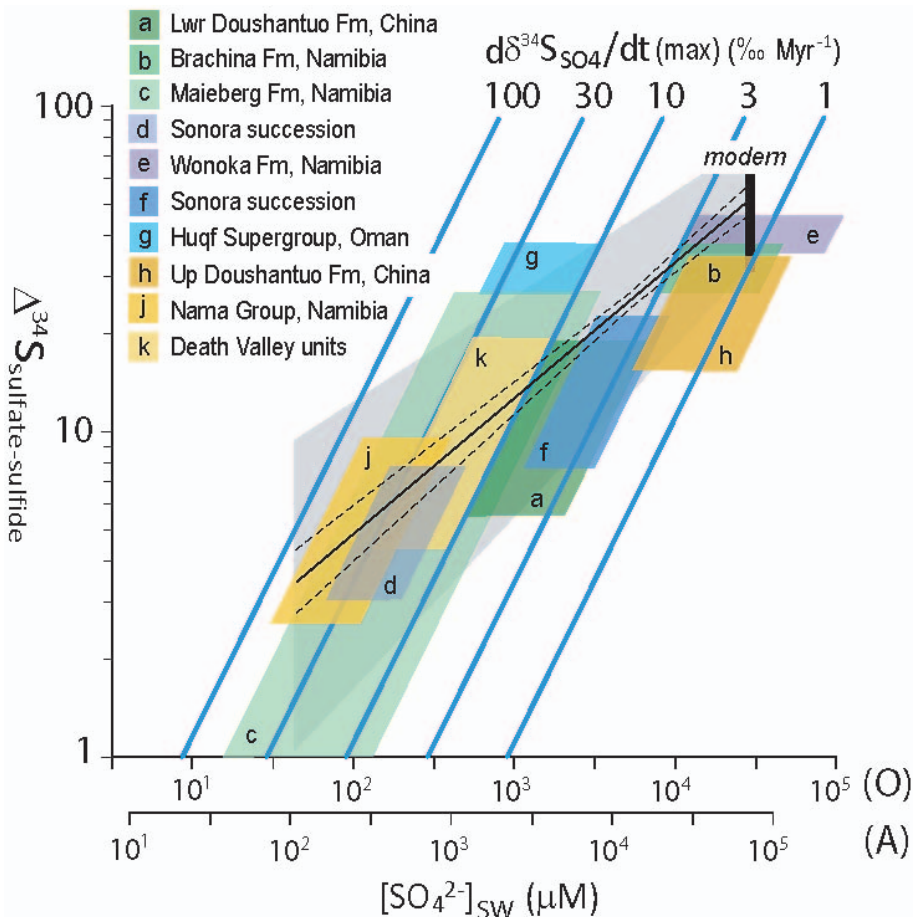


Figure 6. Analysis of seawater sulfate concentrations for 10 Neoproterozoic marine units. The parallelogram for each unit was generated using the rate method. Data sources are given in Table A4; other details as in Figs. 1 and 2.

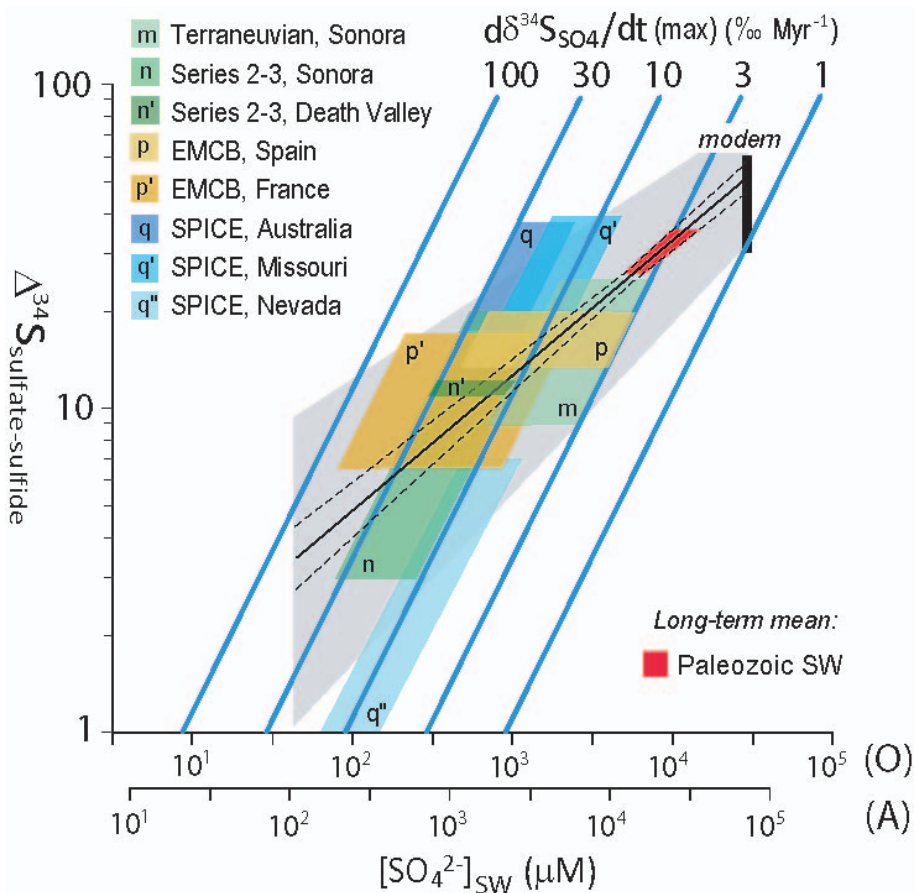


Figure 7. Analysis of seawater sulfate concentrations for 8 Paleozoic marine units. The parallelogram for each unit was generated using the rate method. The red field represents the long-term average $\Delta^{34}\text{S}_{\text{CAS-PY}}$ for the Paleozoic based on data in Wu et al. (2010). Data sources are given in Table A4; other details as in Figs. 1 and 2.

Reconstruction of seawater sulfate

T. J. Algeo et al.

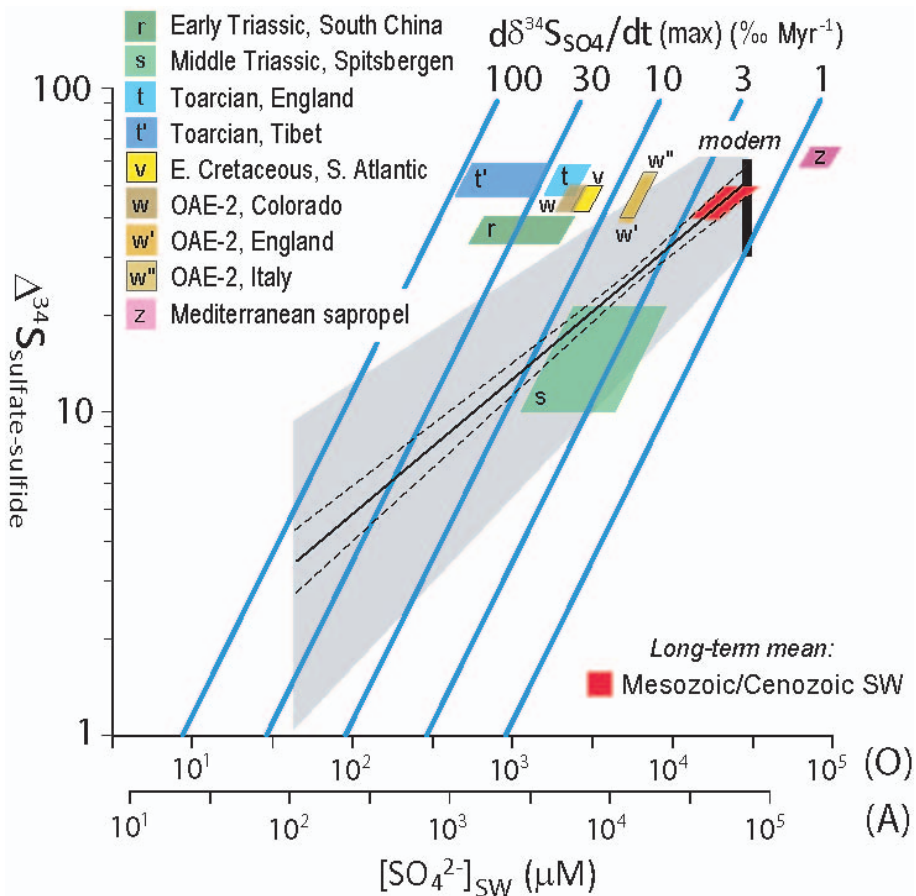


Figure 8. Analysis of seawater sulfate concentrations for 8 Mesozoic–Cenozoic marine units. The parallelogram for each unit was generated using the rate method. The red field represents the long-term average $\Delta^{34}\text{S}_{\text{CAS-PY}}$ for the Mesozoic–Cenozoic based on data in Wu et al. (2010). Data sources are given in Table A4; other details as in Figs. 1 and 2.

Discussion Paper | Reconstruction of seawater sulfate

T. J. Algeo et al.

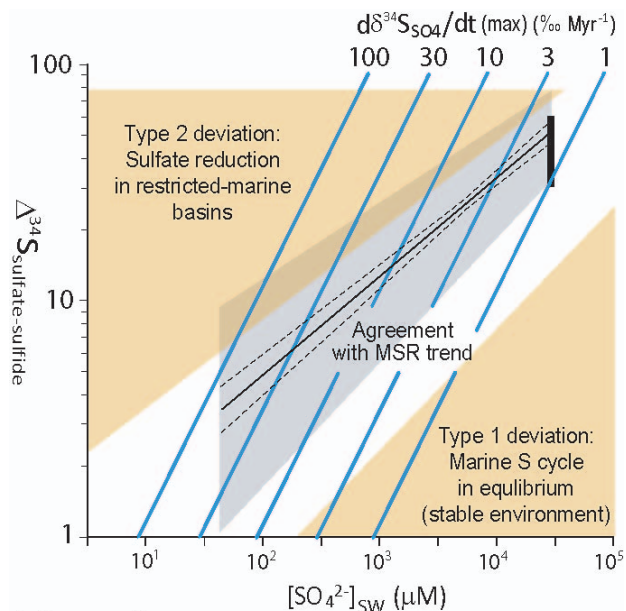


Figure 9. Interpretation of deviations of rate-based $[SO_4^{2-}]$ estimates from MSR-trend-based $[SO_4^{2-}]$ estimates. Type 1 deviations, in which rate-based estimates are anomalously high (lower right field), are likely to reflect extremely stable environmental conditions, in which the marine sulfur cycle is in equilibrium (i.e., balanced source and sink fluxes). Type 2 deviations, in which rate-based estimates are anomalously low (upper left field), are likely to reflect sulfate reduction in restricted-marine basins. In this case, $\Delta^{34}S_{CAS-PY}$ will be controlled by $[SO_4^{2-}]_{sw}$, which may be equal or close to that of the global ocean, but $\partial \delta^{34}S_{CAS} / \partial t(\text{max})$ will be controlled by the mass of aqueous sulfate within the restricted basin, which will be a function of basin volume.

Title Page	Abstract	Introduction
Conclusions	References	
Tables	Figures	
◀	▶	
◀	▶	
Back	Close	
Full Screen / Esc		
Printer-friendly Version		
Interactive Discussion		



Reconstruction of seawater sulfate

T. J. Algeo et al.

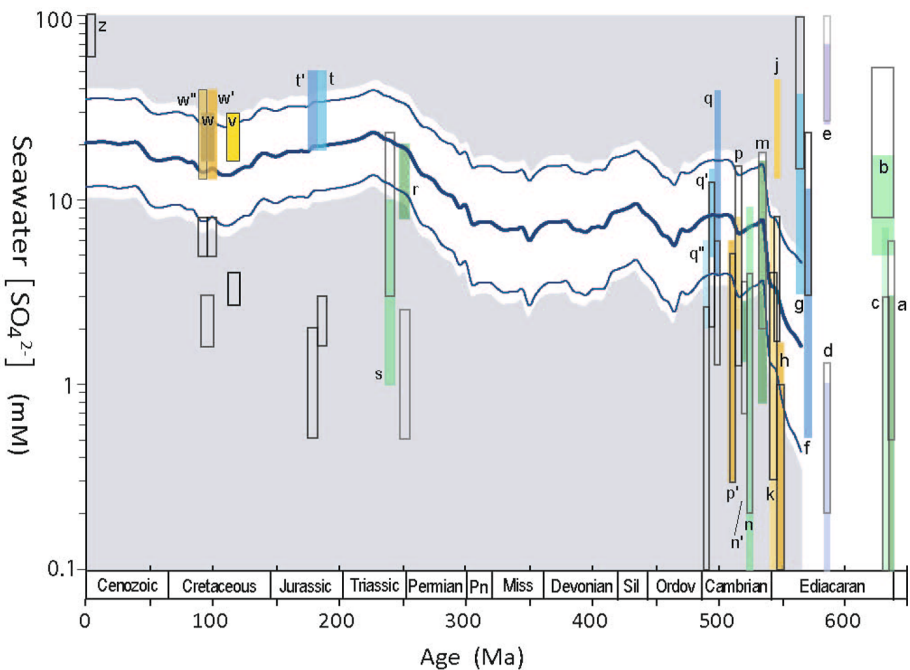


Figure 10. Seawater sulfate concentrations for Neoproterozoic and Phanerozoic marine units (Figs. 6–8) compared with long-term $[\text{SO}_4^{2-}]_{\text{SW}}$ curve (Fig. 4). Estimates of $[\text{SO}_4^{2-}]_{\text{SW}}$ are based on (1) the rate method (calculated per Eqs. 3 and 4; shown as open boxes) and (2) the MSR-trend method (calculated per Eqs. 6–8; shown as colored boxes); note that unit symbols and colors are keyed to Table A4 and Figs. 6–8. See text for discussion. Other details as in Fig. 4.

- [Title Page](#)
- [Abstract](#) [Introduction](#)
- [Conclusions](#) [References](#)
- [Tables](#) [Figures](#)
- [◀](#) [▶](#)
- [◀](#) [▶](#)
- [Back](#) [Close](#)
- [Full Screen / Esc](#)
- [Printer-friendly Version](#)
- [Interactive Discussion](#)

